Molecular Psychiatry
https://doi.org/10.1038/s41380-021-01175-1

ARTICLE

Reversing frontal disinhibition rescues behavioural deficits in models of *CACNA1A*-associated neurodevelopment disorders

Alexis Lupien-Meilleur[1,2] · Xiao Jiang[1,2] · Mathieu Lachance[1] · Vincent Taschereau-Dumouchel[3] · Louise Gagnon[3] · Catherine Vanasse[3] · Jean-Claude Lacaille[2] · Elsa Rossignol[1,2,3]

Received: 20 March 2020 / Revised: 27 April 2021 / Accepted: 12 May 2021

Abstract

CACNA1A deletions cause epilepsy, ataxia, and a range of neurocognitive deficits, including inattention, impulsivity, intellectual deficiency and autism. To investigate the underlying mechanisms, we generated mice carrying a targeted *Cacna1a* deletion restricted to parvalbumin-expressing (PV) neurons (PV^{Cre};$Cacna1a^{c/+}$) or to cortical pyramidal cells (PC) ($Emx1^{Cre}$;$Cacna1a^{c/+}$). GABA release from PV-expressing GABAergic interneurons (PV-INs) is reduced in PV^{Cre};$Cacna1a^{c/+}$ mutants, resulting in impulsivity, cognitive rigidity and inattention. By contrast, the deletion of *Cacna1a* in PCs does not impact cortical excitability or behaviour in $Emx1^{Cre}$;$Cacna1a^{c/+}$ mutants. A targeted *Cacna1a* deletion in the orbitofrontal cortex (OFC) results in reversal learning deficits while a medial prefrontal cortex (mPFC) deletion impairs selective attention. These deficits can be rescued by the selective chemogenetic activation of cortical PV-INs in the OFC or mPFC of PV^{Cre};$Cacna1a^{c/+}$ mutants. Thus, *Cacna1a* haploinsufficiency disrupts perisomatic inhibition in frontal cortical circuits, leading to a range of potentially reversible neurocognitive deficits.

Introduction

Missense mutations in the *CACNA1A* gene, encoding the α1 subunit of the voltage-gated P/Q-type calcium channel $Ca_V2.1$, cause episodic ataxia type 2 (EA2) or familial hemiplegic migraine type 1 (FHM1) by inducing, respectively, either a loss- or a gain-of-function of the gene [1]. Growing evidence suggest that *CACNA1A* loss-of-function (LOF) mutations cause extra-cerebellar phenotypes, including epilepsy and cognitive impairment [2–7]. We recently described that *CACNA1A* LOF mutations, such as deletions and stop gain mutations, result in epileptic encephalopathy with generalized seizures or susceptibility to febrile seizures, mild EA2 with downbeat nystagmus, and a spectrum of cognitive-behavioural deficits ranging from learning disabilities, inattention (ADD), intellectual deficiency (ID) and/or autism spectrum disorder (ASD) [2]. However, the extent of the neurobehavioural impairments associated with *CACNA1A* LOF mutations has not been fully described to date and the underlying mechanisms are unknown.

$Ca_V2.1$ channels regulate pre-synaptic calcium entry and neurotransmitter release at a variety of central synapses, including in cortical, hippocampal and cerebellar circuits [8]. Although the loss of $Ca_V2.1$ channels can be compensated by an up-regulation of other voltage-gated calcium channels at most central synapses [9], this compensation is insufficient to rescue neurotransmission from specific cell types, resulting in clinical deficits. For instance, we recently showed that the selective ablation of *Cacna1a* in cortical GABAergic interneurons suffices to induce generalized epilepsy in mice, and that $Ca_V2.1$ channels are critical to ensure reliable neurotransmission from parvalbumin-positive (PV) cortical fast-spiking GABAergic interneurons (INs) but that they are dispensable at synapses formed by somatostatin-positive INs [10, 11] (SST). In addition, we showed that the homozygous loss of *Cacna1a* at glutamatergic synapses reduces cortical excitability

Supplementary information The online version contains supplementary material available at https://doi.org/10.1038/s41380-021-01175-1.

✉ Elsa Rossignol
elsa.rossignol@umontreal.ca

[1] CHU Ste-Justine Research Center, Montreal, QC, Canada

[2] Department of Neurosciences, U. de Montreal, Montreal, QC, Canada

[3] Department of Pediatrics, U. de Montreal, Montreal, QC, Canada

Published online: 14 June 2021

without an apparent clinical phenotype, but that it lessens the seizure severity when combined with a targeted deletion in cortical INs [10]. Together, our data suggested that cortical disinhibition due to synaptic failure of PV-INs underlies the seizure disorder in mutant mice with *Cacna1a* LOF mutations.

Dysfunction of cerebellar circuits results in a range of motor symptoms, including nystagmus, ataxia and impaired coordination [12–14], and might contribute to some aspects of the cognitive-behavioural phenotype associated with *CACNA1A* LOF. However, a growing body of literature also illustrates the role of PV-INs in cognitive functions, including in cortical sensory processing, attention, cognitive flexibility and working memory [15–23]. We thus hypothesized that cortical disinhibition might contribute to the cognitive deficits associated with *CACNA1A* LOF.

In this paper, we describe the extent of the neurocognitive deficits in patients with *CACNA1A* haploinsufficiency. Further, we dissect the impact of *Cacna1a* haploinsufficiency in various neuronal populations in mice. We demonstrate that a targeted *Cacna1a* deletion in PV-INs induces deficits in selective attention and cognitive flexibility by impairing synaptic release from PV-INs, while a deletion in pyramidal cells (PC) has no apparent behavioural or functional consequences. Further, we show that a targeted deletion of *Cacna1a* in the medial prefrontal cortex (mPFC) impairs selective attention while a deletion in the orbitofrontal cortex (OFC) induces cognitive rigidity. Importantly, these deficits can be rescued by a targeted chemogenetic activation of PV-INs in the mPFC or OFC respectively. Thus, deficits in selective attention and in cognitive flexibility are attributable to a disinhibition of frontal circuits in *Cacna1a* conditional mutants, which can be reversed by a targeted activation of PV-INs in mature circuits.

Results

Neuropsychological deficits in patients carrying *CACNA1A* LOF mutations

We previously reported the clinical phenotype of 16 patients from 4 different families carrying *CACNA1A* LOF mutations [2]. Most patients in this cohort presented some degree of cognitive and/or behavioural impairment, ranging from learning disability and ADHD, to autism or ID, together with mild episodic ataxia (EA2) and interictal down-beat nystagmus [2]. To better characterize the neurocognitive deficits associated with *CACNA1A* haploinsufficiency, we conducted formal neuropsychological evaluations of all 6 children in this cohort. We observed reduced global IQ (WISC-IV, Fig. 1a), as well as inattention and learning impairments (Conner's scale, Fig. 1b) despite treatment with psychostimulants. Further, we observed

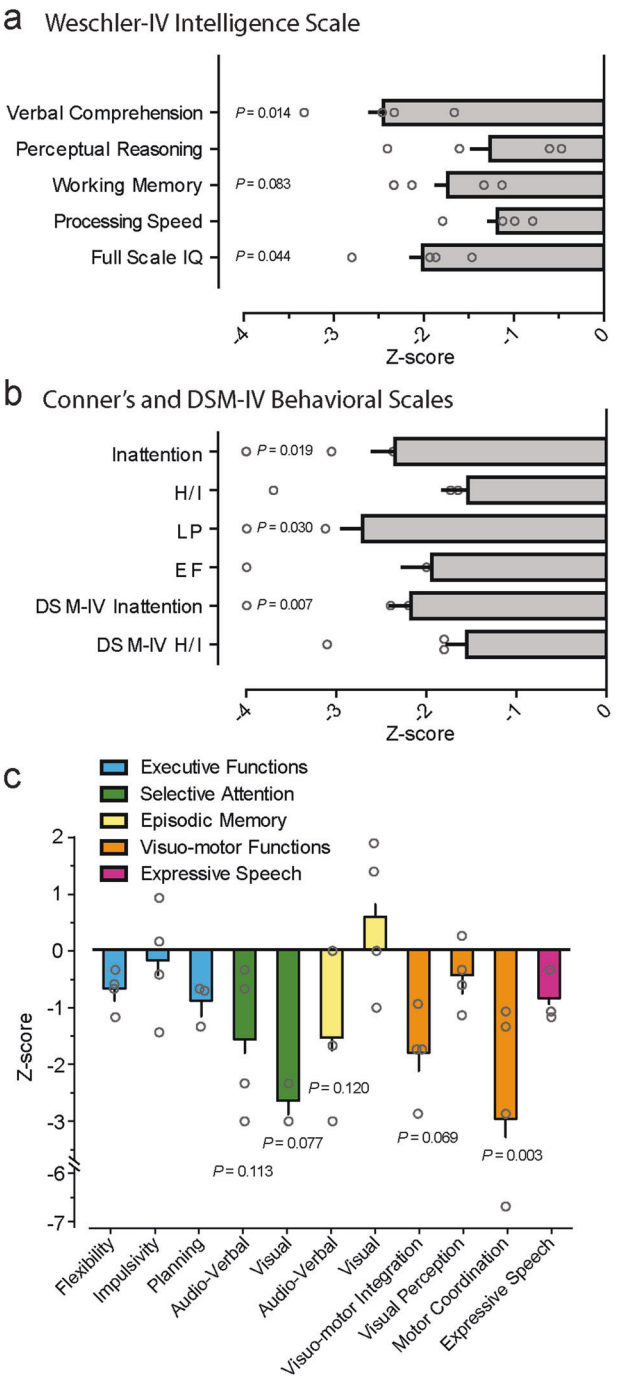

Fig. 1 Neurocognitive deficits in patients with *CACNA1A* haploinsufficiency. a Cognitive assessments using the Weschler-IV Intelligence Scale in children with *CACNA1A* haploinsufficiency revealed reduced global IQ, with significant deficits in working memory and verbal comprehension. **b** The Conner's and the DSM-IV Behavioural Scales unveiled significant attention and learning deficits (H/I hyperactivity/impulsivity, LP learning problems, EF executive function). **c** Extensive neuropsychological testing highlighted deficits in selective attention, audio-verbal memory and visuo-motor functions.

striking deficits in various neuropsychological functions, including deficits in selective attention, speech comprehension, working memory and verbal encoding (Fig. 1c); as well as

impaired fine motor skills, bimanual coordination and visuo-constructive abilities (Fig. 1c).

Decreased perisomatic inhibition in the frontal cortex of PV^{Cre};$Cacna1a^{c/+}$ mutant mice

The impairments in selective attention and executive functions observed in patients with *CACNA1A* haploinsufficiency suggest an underlying dysfunction of frontal cortical circuits. Given the critical role of $Ca_V2.1$ in regulating synaptic release from cortical PV-INs [10, 24], and the implication of PV-INs in cognition and behaviour [20, 21, 23, 25], we postulated that the neurobehavioural deficits observed in patients may result from impaired PV-IN mediated inhibition in frontal cortical circuits. To study this possibility in an animal model of the disorder, we generated conditional PV^{Cre};$Cacna1a^{c/+}$ mutant mice carrying a targeted heterozygote *Cacna1a* deletion in PV-expressing neurons. The PV^{Cre} allele is expressed progressively in S1 cortical PV-INs from P14 onwards, with maximal recombination by P30 [11]. We observed similar high recombination rates of the PV^{Cre} allele in frontal cortical areas, with the Cre recombinase being expressed in most PV-INs at P30, with a high specificity for PV-expressing neurons (Supplementary Fig. 1a–e).

Mutant PV^{Cre};$Cacna1a^{c/+}$ mice do not display gross motor deficits (i.e. ataxia or dystonia), spontaneous seizures or interictal epileptic activity on 72 h video-EEG recordings ($n = 8$) (Supplementary Fig. 2a, b). Notably, no seizures or spontaneous epileptic activity occurred during daily handling by animal caretakers or when the animals were exploring the recording arena. However, the PV^{Cre};$Cacna1a^{c/+}$ mice show a reduced seizure threshold to Pentylenetetrazol (PTZ)-induced seizures, suggesting an increased seizure susceptibility (Fig. 2a).

To investigate the impact of *Cacna1a* haploinsufficiency on fronto-cortical PV-INs, we recorded light-evoked inhibitory post-synaptic currents (IPSCs) in deep-layer PCs of the OFC or mPFC in acute cortical slices of PV^{Cre};$Cacna1a^{c/+}$ mutants compared to PV^{Cre} control littermates at P60; 2 weeks after injecting a Cre-dependent AAV9.CAGGS.Flex.ChR2-tdTomato.WPRE.SV40 virus. Only slices with similar significant levels of tdTomato expression were selected for experiments, and no differences were noted in tdTomato expression in PV^{Cre};$Cacna1a^{c/+}$ mutant and PV^{Cre} control mice. The optogenetic stimulation of PV-INs revealed smaller light-evoked IPSCs in PV^{Cre};$Cacna1a^{c/+}$ mutants compared to PV^{Cre} control littermates, suggesting a profound deficit in synaptic GABA release from PV-INs (Fig. 2b, c), despite preserved numbers and distribution of PV-INs (Supplementary Fig. 1b).

To further characterize the synaptic dysfunction of fronto-cortical PV-INs, we recorded unitary IPSCs (uIPSCs) in paired whole-cell recordings between PV-INs and deep-layer PCs in mPFC slices of PV^{Cre};$Cacna1a^{c/+}$;$RCE^{EGFP/+}$ mutants and PV^{Cre};$RCE^{EGFP/+}$ littermates. We observed a reduced release probability and decreased paired-pulse ratio (Fig. 2d), suggesting a reduction in the reliability of synaptic transmission from PV-INs. Further, PV-PC uIPSCs were of lower amplitude, shorter duration, and showed decreased total charge and slower rise time, compatible with a presynaptic impairment of GABA release (Fig. 2d), as previously observed with homozygous deletions of *Cacna1a* [10, 11].

Reduced anxiety in PV^{Cre};$Cacna1a^{c/+}$ mutants

We next characterized the impact of the targeted haploinsufficiency of *Cacna1a* in PV neurons on mouse behaviour and cognition. In the Open Field, PV^{Cre};$Cacna1a^{c/+}$ mutant mice spent more time than controls in the central zone of the maze (Fig. 2e), suggesting a reduction in anxiety-related behaviours. However, they did not show hyperactivity as they travelled similar distances at similar speed compared to their control littermates (Fig. 2e). In the Elevated Plus Maze, PV^{Cre};$Cacna1a^{c/+}$ mutant mice explored the open arms more than the controls (Fig. 2f), again suggesting a reduction in anxiety-driven behaviour.

PV^{Cre};$Cacna1a^{c/+}$ mutants display deficits in socialization but not in novelty-seeking

Dysfunction of fronto-cortical PV-IN has been postulated to contribute to the socialization deficits in patients with autism and in mice models of the disease [26]. Interestingly, PV^{cre};$Cacna1a^{c/+}$ mutants showed deficits in social interactions in the three chamber maze: they spent more time in the chamber with the empty cage than in the chamber with a stranger mouse (S1)(Fig. 2g). However, they exhibited normal social novelty-seeking behaviours: they spent more time in the chamber with a novel mouse (S2) than in the chamber with a known mouse (S1), similar to controls (Fig. 2g).

PV^{Cre};$Cacna1a^{c/+}$ mutants display deficits in reversal learning and in selective attention

Given the importance of hippocampal PV-INs in learning and memory [21, 27], we tested PV^{Cre};$Cacna1a^{c/+}$ mice for hippocampal-based cognitive impairments. We found no difference between PV^{Cre};$Cacna1a^{c/+}$ mutants and their control littermates in the novel object recognition task or in the displaced object recognition task (Fig. 2h). Furthermore, PV^{Cre};$Cacna1a^{c/+}$ mice performed as well as their control littermates in the learning phase of the Morris Water Maze task, a well-established spatial learning and memory task (Fig. 2i). A probe test 24 h after the 5th day of the task also

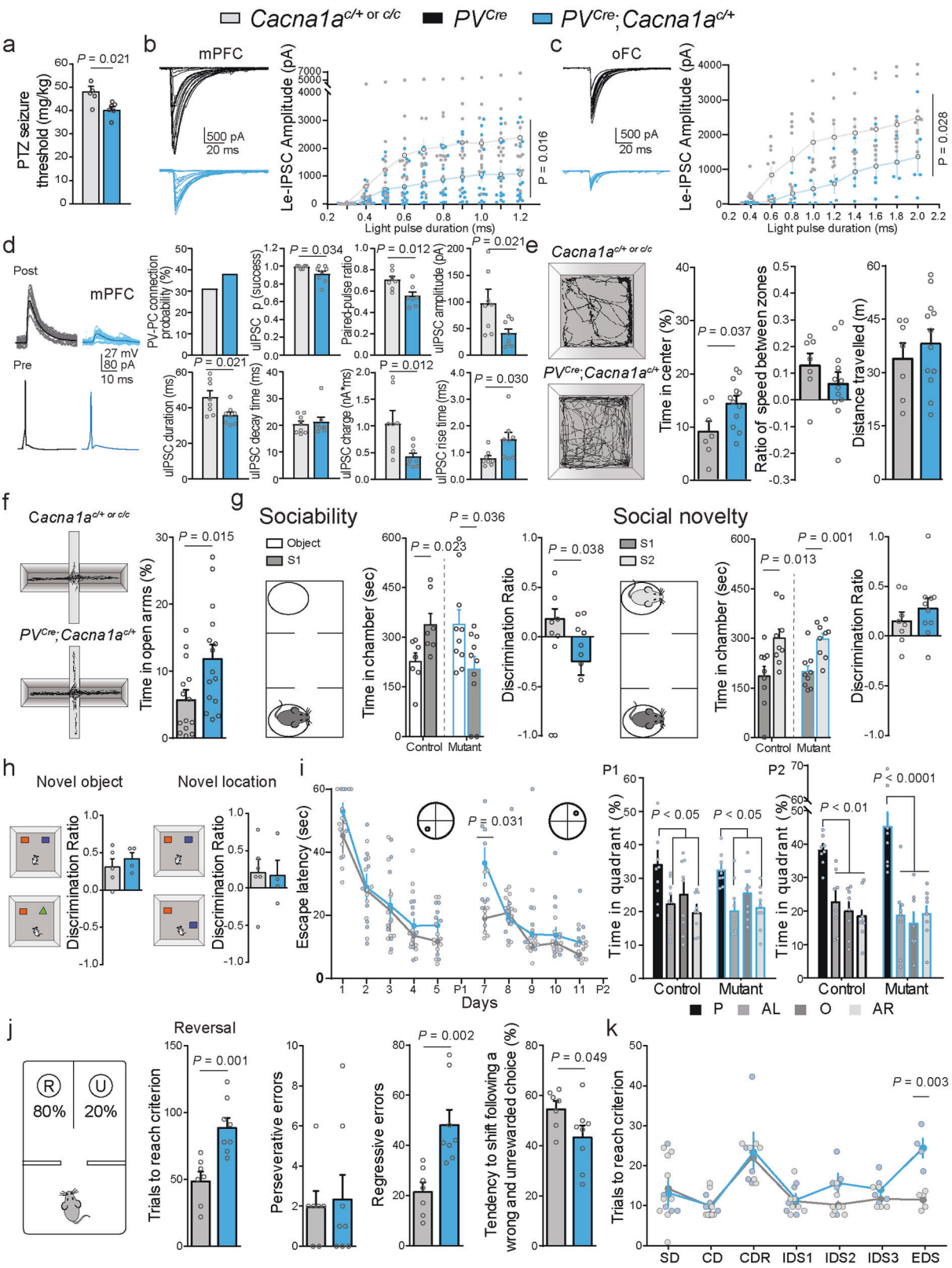
Cacna1a c/+ or c/c
PVCre
PVCre;Cacna1a c/+
a
PTZ seizure threshold (mg/kg)
P = 0.021
b
mPFC
500 pA
20 ms
Le-IPSC Amplitude (pA)
P = 0.016
Light pulse duration (ms)
c
oFC
500 pA
20 ms
Le-IPSC Amplitude (pA)
P = 0.028
Light pulse duration (ms)
d
Post
mPFC
Pre
27 mV
80 pA
10 ms
PV-PC connection probability (%)
uIPSC p (success)
P = 0.034
Paired-pulse ratio
P = 0.012
uIPSC amplitude (pA)
P = 0.021
uIPSC duration (ms)
P = 0.021
uIPSC decay time (ms)
uIPSC charge (nA*ms)
P = 0.012
uIPSC rise time (ms)
P = 0.030
e
Cacna1a c/+ or c/c
PVCre;Cacna1a c/+
Time in center (%)
P = 0.037
Ratio of speed between zones
Distance travelled (m)
f
Cacna1a c/+ or c/c
PVCre;Cacna1a c/+
Time in open arms (%)
P = 0.015
g
Sociability
Object
S1
Time in chamber (sec)
P = 0.023
P = 0.036
Discrimination Ratio
P = 0.038
Control
Mutant
Social novelty
S1
S2
Time in chamber (sec)
P = 0.013
P = 0.001
Discrimination Ratio
Control
Mutant
h
Novel object
Discrimination Ratio
Novel location
Discrimination Ratio
i
Escape latency (sec)
P = 0.031
Days
P1
P2
Time in quadrant (%)
P < 0.05
P < 0.05
Control
Mutant
P2
Time in quadrant (%)
P < 0.01
P < 0.0001
Control
Mutant
P
AL
O
AR
j
R
U
80%
20%
Reversal
Trials to reach criterion
P = 0.001
Perseverative errors
Regressive errors
P = 0.002
Tendency to shift following a wrong and unrewarded choice (%)
P = 0.049
k
Trials to reach criterion
P = 0.003
SD
CD
CDR
IDS1
IDS2
IDS3
EDS

◀ **Fig. 2 *Cacna1a* haploinsufficiency in PV-INs reduces synaptic inhibition and leads to decreased anxiety, reversal learning deficits and selective attention deficits. a** Mutant mice show an increased sensitivity to PTZ-induced seizures, with reduced seizure threshold at P60 ($n = 5$ controls, 6 mutants PV^{Cre};$Cacna1a^{c/+}$). **b**, **c** Representative traces (left) and summary graph (right) of input-output function of light-evoked IPSCs from PV-INs onto deep-layer PC of control (PV^{Cre}) and mutant PV^{Cre};$Cacna1a^{c/+}$ mice in (**b**) mPFC ($n = 12$ cells/3 mice in controls, $n = 14$ cells/3 mice in PV^{Cre};$Cacna1a^{c/+}$) and (**c**) OFC (OFC: $n = 9$ cells/4 mice in control, and $n = 5$ cells/4 mice in PV^{Cre};$Cacna1a^{c/+}$), suggesting a reduction in synaptic transmission from PV-INs (**d**). Representative traces (left) and summary graphs (right) of properties of unitary IPSCs from paired recordings between PV-INs and deep-layer PC in the mPFC showing a reduced probability of successful transmission, decreased paired-pulse ratio, reduced amplitude and charge transfer, and altered uIPSC kinetics (reduced duration and increased rise time) in PV^{Cre};$Cacna1a^{c/+}$ mice compared to controls ($n = 8$ connected pairs of 28 tested pairs in 6 control mice; $n = 8$ connected pairs of 21 tested pairs in 7 mutant PV^{Cre};$Cacna1a^{c/+}$ mice). (**e**) Open Field; illustrative examples of travel paths from control (top) and mutant (bottom) mice ($n = 7$ controls, $n = 12$ PV^{Cre};$Cacna1a^{c/+}$ mutants). Mean time spent in the central zone of the Open Field (left), ratio of the speed in the centre zone compared to the periphery (middle) and total distance travelled (right). **f** Elevated Plus Maze; representative paths taken by controls (top) and PV^{Cre};$Cacna1a^{c/+}$ (bottom) mice in the Elevated Plus Maze with time spent on the open arms of the maze ($n = 12$ controls, $n = 15$ PV^{Cre};$Cacna1a^{c/+}$ mutants). **g** Social Novelty test ($n = 8$ controls, $n = 10$ PV^{Cre};$Cacna1a^{c/+}$ mutants); sociability preferences (left): time spent with an empty cage (white) and with a mouse (Stranger 1, S1; dark grey) in the three chamber maze (left); and discrimination ratio (time spent with the mice compared to the time spent with the inanimate object). Preference for social novelty (right): time spent with S1 (dark grey) and a new mouse (S2; light grey) (left). Discrimination ratio of the time spent with the novel mouse compared to the time spent with the known mouse. **h** Object novelty (left): ratio of the time spent with a novel object compared to time spent with a known object. Novel location (right): ratio of the time spent with a displaced object compared to time spent with the object in the initial location ($n = 6$ controls, $n = 4$ PV^{Cre};$Cacna1a^{c/+}$ mutants). **i** Morris Water Maze: learning curve in the Morris Water Maze task (left), with reversal on day 7 (inserts depict the localisation of the platform). Probe test (right): probe tests are conducted on day 6 and day 12 (P: platform; AL: adjacent left; O: opposite; AR: adjacent right; P1: probe test 1; P2: probe test 2) ($n = 6$ controls, $n = 9$ PV^{Cre};$Cacna1a^{c/+}$ mutants). **j** Probabilistic reversal learning task: diagram of the maze (left) showing a reward-containing well (R) and an unrewarded empty well (U). Number of trials needed to reach criterion in the reversal step, the number of perseverative errors (second graph), the number of regressive errors (third graph) and the shifting behaviour (fourth graph) ($n = 7$ controls, $n = 8$ PV^{Cre};$Cacna1a^{c/+}$ mutants). **k** Attention set shifting task: number of trials needed to reach criterion in the different steps of the task (SD: simple discrimination; CD: compound discrimination; CDR: compound discrimination (reversal); IDS1-3: intra-dimensional shift 1 to 3; EDS: extra-dimensional shift) ($n =$ 5 control, 5 PV^{Cre};$Cacna1a^{c/+}$ mutants). Error bars represent mean ± s.e.m. Two-tailed Student's *t* test was conducted in **a**, **d**, **e**, **f**, **g**, **h**, **i** (day7), **j**. Two-way ANOVA repeated measure with Bonferroni's t-test was conducted in **b**, **i**. Two-way ANOVA with Bonferroni's t-test was conducted in **g**, **h**, **i** (probe test) and **k**.

showed intact spatial memory formation (Fig. 2i). However, PV^{Cre};$Cacna1a^{c/+}$ mutant mice displayed a reversal learning deficit when the platform was displaced to the opposite quadrant on the 7th day (Fig. 2i). The mutant mice eventually learned the new rule, as demonstrated by their performance in subsequent days, and they were able to form a proper spatial memory of the novel platform location, as shown by the second probe test (Fig. 2i). Together, these results suggest a relative preservation of hippocampal functions in PV^{Cre};$Cacna1a^{c/+}$ mutant mice, with intact spatial memory and novel object recognition abilities, but deficits in cognitive flexibility with impaired reversal learning.

To further characterize this reversal learning deficit, we used a stringent probabilistic reversal learning task in which food-deprived animals must identify the well in which a reward is most likely to be found (80% of the time), and then learn to explore the opposite well in the reversal learning task [28]. PV^{Cre};$Cacna1a^{c/+}$ mutant mice showed significant reversal learning deficits: they required more trials than controls to reach criterion (Fig. 2j), and they displayed more regressive errors while learning the new rule, i.e. they reverted to the previous well, even after having been rewarded for exploring the correct well (Fig. 2j). Furthermore, following an unrewarded incorrect choice, mutant mice were more prone to revisit the same side on the following trial compared to controls (Fig. 2j).

PV^{Cre};$Cacna1a^{c/+}$ mutants also display deficits in selective attention, as assessed with an attention set-shifting task [29]. Briefly, the animals explore food wells filled with textured digging materials of different odours. The animals must first learn to discriminate between different textures through four intra-dimensional shift tasks (IDS), and are then required to discriminate between different odours in an extra-dimensional shift task (EDS) (Supplementary Fig. 3a). PV^{Cre};$Cacna1a^{c/+}$ mice displayed clear attention set-shifting deficits as they required significantly more trials to complete the EDS task (Fig. 2k). This is not the result of an olfaction deficit as the mutants performed as well as controls in simple olfactory tests (Supplementary Fig. 3c).

Cacna1a haploinsufficiency does not impair cortical glutamatergic synaptic transmission

We previously demonstrated that the targeted homozygous deletion of *Cacna1a* in cortical PCs decreases cortical excitability in $Emx1^{Cre}$;$Cacna1a^{c/c}$ mutants, presumably by impairing glutamate release [10], as reported also by others [30, 31]. To test whether the heterozygous loss of *Cacna1a* restricted to cortical and hippocampal PCs could also contribute to impairments in behaviour or cognition, we generated the $Emx1^{Cre}$;$Cacna1a^{c/+}$ mutant mice. The $Emx1^{Cre}$ selectively recombines glutamatergic cells in the cortex, sparing GABAergic INs [32]. Surprisingly, we found that the heterozygous loss of *Cacna1a* did not affect glutamatergic synaptic transmission measured with whole-cell recordings in layer V PCs of the OFC. We found no

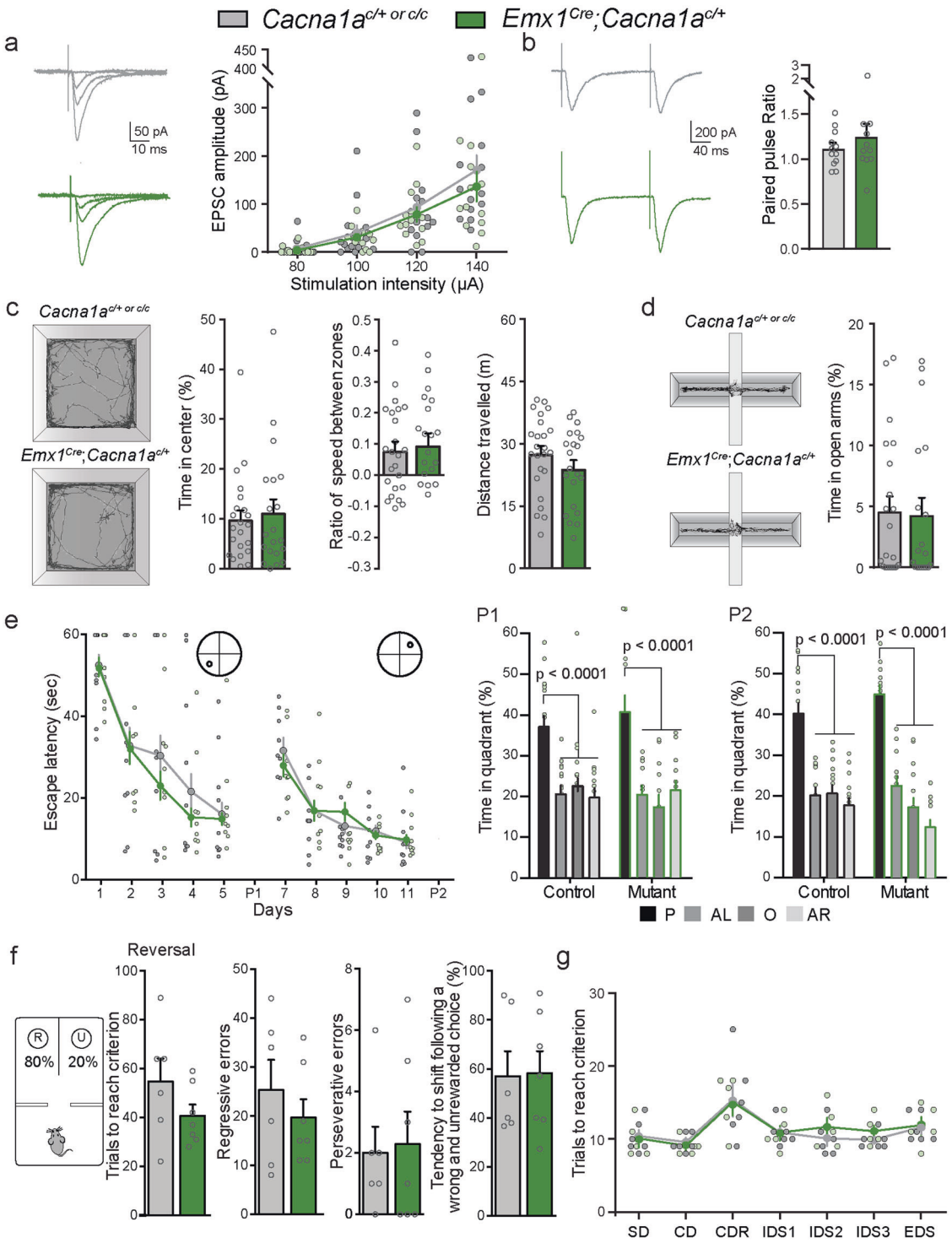

difference in the input-output function of EPSCs evoked by electrical stimulation in OFC slices from of *Emx1*^{Cre}*;Cacna1a*$^{c/+}$ mutants compared to control mice (Fig. 3a). Paired-pulse ratio of excitatory responses was also similar between both groups (Fig. 3b). Furthermore, *Emx1*^{Cre}*;Cacna1a*$^{c/+}$ mice showed no differences in behaviour in the Open Field (Fig. 3c), the Elevated Plus Maze (Fig. 3d), the Morris Water Maze (including the reversal phase) (Fig. 3e), the probabilistic learning reversal task (Fig. 3f) or in the attention set-shifting task (Fig. 3g) compared to their littermate controls. Overall, these results suggest that the haploinsufficiency of *Cacna1a* selectively impairs cortical inhibitory signalling and that it does not affect cortical glutamatergic transmission.

◀ **Fig. 3 Haploinsufficiency of *Cacna1a* in pyramidal cells does not affect excitatory synaptic transmission in the frontal cortex and does not induce apparent behavioural deficits. a** Representative traces (left) and summary plots (right) of the input-output function of EPSCs evoked by electrical stimulations in whole-cell recordings from PC in OFC slices of control and $Emx1^{Cre}$;$Cacna1a^{c/+}$ mice ($n = 14$ cells/5 mice in controls and 13 cells/3 mice in $Emx1^{Cre}$;$Cacna1a^{c/+}$). **b** Representative traces (left) and summary graph (right) of paired pulse ratio (120 µA stimulation; $n = 12$ cells/5 mice in control and 11 cells/3 mice in $Emx1^{Cre}$;$Cacna1a^{c/+}$). **c** Open field: illustrative travel paths of control mice (top) and $Emx1^{Cre}$;$Cacna1a^{c/+}$ mutants (bottom). Mean time spent in the central zone of the Open field (left) ($n = 22$ controls, $n = 20$ $Emx1^{Cre}$;$Cacna1a^{c/+}$ mutants), ratio of the speed in the centre compared to the periphery (middle) ($n = 24$ controls, $n = 20$ $Emx1^{Cre}$;$Cacna1a^{c/+}$ mutants) and total distance travelled (right) ($n = 24$ controls, $n = 20$ $Emx1^{Cre}$;$Cacna1a^{c/+}$ mutants). **d** Elevated Plus Maze: representative paths taken by controls (top) and $Emx1^{Cre}$;$Cacna1a^{c/+}$ mice (bottom) in the Elevated Plus Maze, with time spent on the open arms of the maze ($n = 21$ controls, $n = 19$ $Emx1^{Cre}$;$Cacna1a^{c/+}$ mutants). **e** Morris Water Maze: learning curve in the Morris Water Maze (left), with a reversal task on day 7 (inserts depict the localisation of the platform). Probe test (right): Probe tests are conducted on day 6 and day 12 (P: platform; AL: adjacent left; O: opposite; AR: adjacent right; P1: probe test 1; P2: probe test 2 ($n = 14$ controls, $n = 15$ $Emx1^{Cre}$;$Cacna1a^{c/+}$ mutants). Curves analysed by Two-way ANOVA (repeated measure) followed by Bonferonni's multiple comparisons post-hoc correction. **f** Probabilistic reversal learning task: diagram of the maze (left) showing a reward-containing well (R) and an unrewarded empty well (U). Number of trials needed to reach criterion in the acquisition step (first graph), the number of regressive errors (second graph), the number of perseverative errors (third graph) and the shifting behaviour after an incorrect unrewarded choice (fifth graph) ($n = 6$ controls, $n = 7$ $Emx1^{Cre}$;$Cacna1a^{c/+}$ mutants). **g** Attention set shifting task: number of trials needed to reach criterion in the different steps of the task (SD: simple discrimination; CD: compound discrimination; CDR: compound discrimination (reversal); IDS1-3: intra-dimensional shift 1 to 3; EDS: extra-dimensional shift) ($n = 6$ controls, $n = 5$ mutants). Error bars represent mean ± s.e.m. Two-tailed Student's *t*-test was conducted in **b**, **c**, **d**, **f**. Two-way ANOVA repeated measure with Bonferroni's *t*-test was conducted in **a**, **e**. Two-way ANOVA with Bonferroni's t-test was conducted in **e** (probe test) and **g**. Mann-Whitney test was applied to **b**.

Disinhibition within the medial prefrontal cortex leads to deficits in selective attention

Recent evidence suggests that mPFC PV-INs are essential for attention set-shifting abilities [19, 23, 33]. Since the PV^{Cre} driver allele drives recombination of the $Cacna1a^{c/+}$ allele in various brain regions (cortex, hippocampus, amygdala, striatum, cerebellum), we employed local AAV-mediated Cre delivery (AAV2/9-Cre, Penn Vector Core) in specific frontal cortical areas of $Cacna1a^{c/+}$ mice to generate mutants with spatially restricted deletions. Given that *Cacna1a* haploinsufficiency selectively impairs GABAergic transmission in the cortex (as shown above in the mPFC and OFC), focal cortical *Cacna1a* deletions are expected to result in selective cortical disinhibition, in part through its effect on PV-INs synaptic transmission. We generated mutant mice carrying focal *Cacna1a* deletions in the mPFC by injecting AAV2/9-Cre viruses, at 6 weeks of age, in the mPFC of $Cacna1a^{c/+}$;$RCE^{EGFP/+}$ animal compared to injected $RCE^{EGFP/+}$ controls (Fig. 4a). No difference was observed between injected mutant and control mice in the Openfield (Fig. 4b), the elevated plus maze (Fig. 4c) or the three-chamber maze (Fig. 4d). Notably, the mPFC-Cre-injected mutants performed as well as their control littermates in the Morris Water Maze (Fig. 4e), including in the reversal learning phase, suggesting preserved spatial learning and cognitive flexibility in this model. However, the injected mutant mice presented striking deficits in selective attention, requiring more trials to complete the EDS task in the attention set-shifting task than control littermates (Fig. 4f), similar to what we had observed in PV^{Cre};$Cacna1a^{c/+}$ mutants. Therefore, the haploinsufficiency of *Cacna1a* leads to deficits in selective attention potentially attributable to an impairment of PV-INs-mediated inhibition in the mPFC.

Disinhibition within the orbitofrontal cortex induces cognitive rigidity

Cognitive rigidity can result from an impairment of OFC circuits [34, 35] and has been associated with disrupted development or function of frontal cortical PV-INs [36]. We tested the behavioural impact of a focal *Cacna1a* deletion in the OFC by injecting Cre-expressing AAVs in the OFC of $Cacna1a^{c/+}$;$RCE^{EGFP/+}$ mice or in control $RCE^{EGFP/+}$ mice littermates at 6 weeks of age (Fig. 5a). OFC-Cre-injected $Cacna1a^{c/+}$;$RCE^{EGFP/+}$ mice showed no deficit in the Open Field (Fig. 5b) or the Elevated Plus Maze (Fig. 5c) compared to their control littermates, suggesting that the reduction in anxiety observed in the PV^{Cre};$Cacna1a^{c/+}$ mutant mice is not attributable to a dysfunction of the OFC circuits. Furthermore, the mutant mice performed as well as their control littermates in the learning phase of the Morris Water Maze (Fig. 5d), suggesting preserved spatial learning and memory. However, they displayed reversal learning deficits, reminiscent of those observed in the PV^{Cre};$Cacna1a^{c/+}$ mutant mice. Indeed, in the reversal phase of the MWM, mutant mice took more time to learn the novel position of the moved hidden platform on days 7 and 8 compared to injected controls (Fig. 5d). The mutants progressively learned the new localization and showed a good retention on both probe tests (Fig. 5d), suggesting an intact spatial memory formation.

The probabilistic reversal-learning task confirmed the cognitive flexibility deficits in the OFC-Cre-injected $Cacna1a^{c/+}$ mice during the reversal learning phase (Fig. 5e), similar to what we had observed in PV^{Cre};$Cacna1a^{c/+}$ mutants. The OFC-Cre-injected $Cacna1a^{c/+}$;RCE^{EGFP} mutants made more regressive errors and were significantly more prone to revisit an unrewarded well following an unrewarded incorrect choice (Fig. 5e). However, this mice line performed normally in the attention set-shifting task (Fig. 5f). Taken together, our results suggest that the haploinsufficiency of *Cacna1a* leads to cognitive rigidity (reversal learning deficits) through reduced inhibition of the OFC.

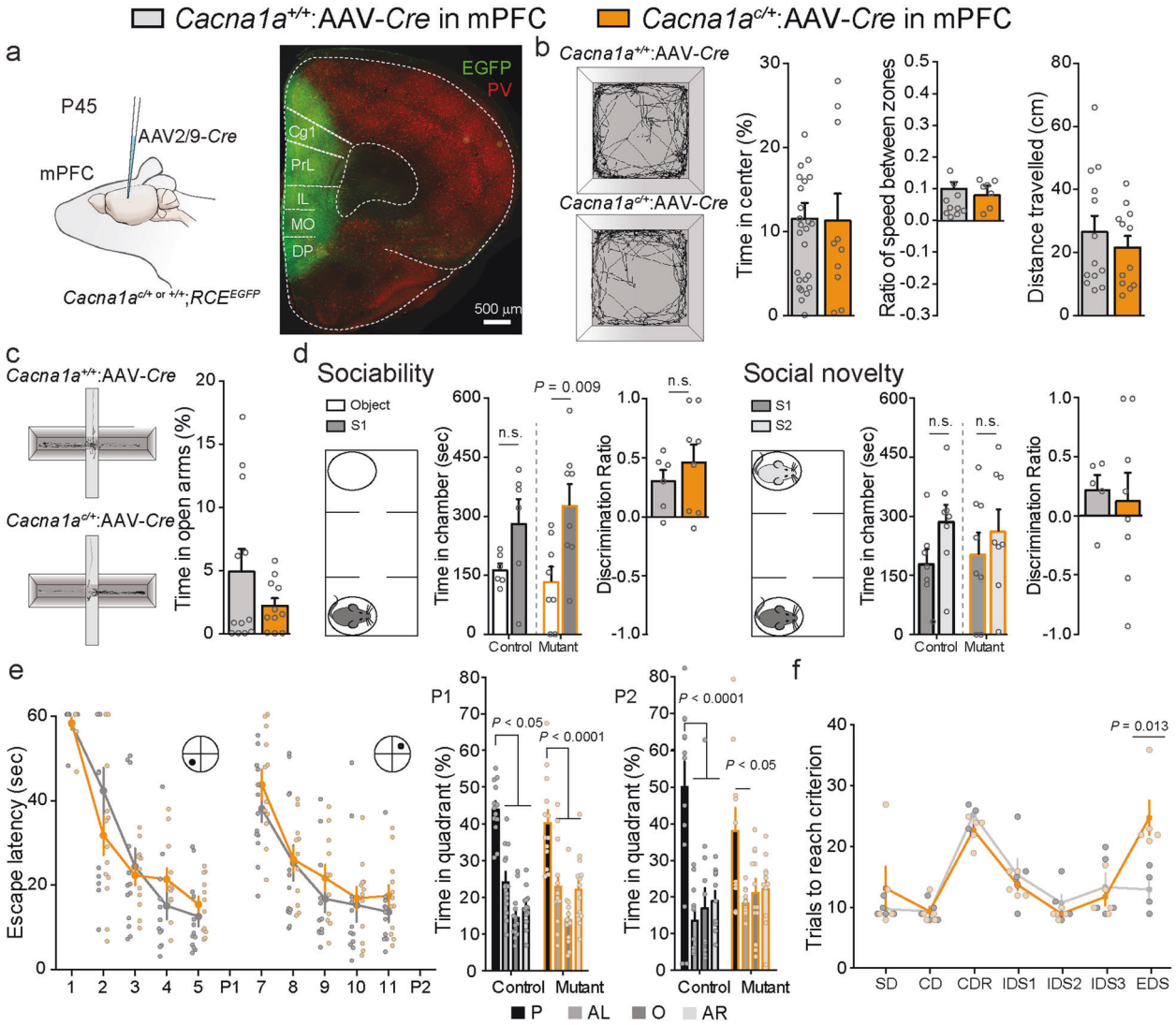

Fig. 4 Selective attention deficits recapitulated by a targeted heterozygous deletion of *Cacna1a* in the mPFC. a The mPFC of *Cacna1a*$^{c/+}$;*RCE*^{EGFP} mutant and *Cacna1a*$^{+/+}$;*RCE*^{EGFP} control mice were injected with an AAV2/9-Cre expressing virus. The infection was restricted to the mPFC as shown by infected cells expressing EGFP. **b** Open field: Illustrative travel path of a control (top) and a mPFC-Cre-injected *Cacna1a*$^{c/+}$ mouse (bottom). Mean time spent in the central zone of the Open field (left), ratio of the speed in centre compared to the periphery (middle) and total distance travelled (right) ($n = 11$ controls, $n = 12$ mutants). **c** Elevated Plus Maze: representative paths taken by control (top) and mPFC-Cre-injected *Cacna1a*$^{c/+}$ mutant mice (bottom) in the Elevated Plus Maze, with time spent on the open arms of the maze ($n = 12$ controls, $n = 11$ mutants). **d** Social Novelty test ($n = 5$ controls, $n = 6$ mutants); sociability preferences (left): time spent with an empty cage (white) and with a mouse (Stranger 1, S1; dark grey) in the three chamber maze (left); and discrimination ratio (time spent with the mice over time spent with the inanimate object). Preference for social novelty (right): time spent with S1 (dark grey) and a new mouse (S2; light grey) (left). Discrimination ratio of the time spent with the novel mouse compared to the time spent with the known mouse (n.s. non significative). **e** Morris Water Maze: learning curve in the Morris Water Maze task (left), with reversal on day 7 (inserts depict the localisation of the platform). Probe test (right): probe tests were conducted on days 6 and 12 (P: platform; AL: adjacent left; O: opposite; AR: adjacent right; P1: probe test 1; P2: probe test 2) ($n = 13$ controls, $n = 12$ mutants). **f** Attention set-shifting task: number of trials needed to reach criterion in the different steps of the task (SD simple discrimination, CD compound discrimination, CDR compound discrimination (reversal), IDS1-3 intra-dimensional shift 1 to 3, EDS extra-dimensional shift) ($n = 5$ controls, $n = 5$ mutants). Error bars represent mean ± s.e.m. Two-tailed Student's t test was conducted in b, c, d. Two-way repeated measure ANOVA with Bonferroni's *t*-test was applied to e. Two-way ANOVA with Bonferroni's t-test was conducted in **e** (probe test) and **f**.

The Targeted chemogenetic activation of mPFC PV-INs rescues the selective attention deficits in *PV*^{Cre};*Cacna1a*$^{c/+}$ mutants

To investigate whether specific aspects of the behavioural deficits observed in *PV*^{Cre};*Cacna1a*$^{c/+}$ mice are indeed attributable to deficits in PV-INs function within the frontal circuits, we examined if the selective chemogenetic activation of PV-INs could rescue the behavioural deficits. We selectively activated PV-INs in the mPFC or OFC of *PV*^{Cre};*Cacna1a*$^{c/+}$ mutants using a Cre-dependent 246-pAAV-hSYN-DIO-hM3D-mCherry virus (Fig. 6a). We first

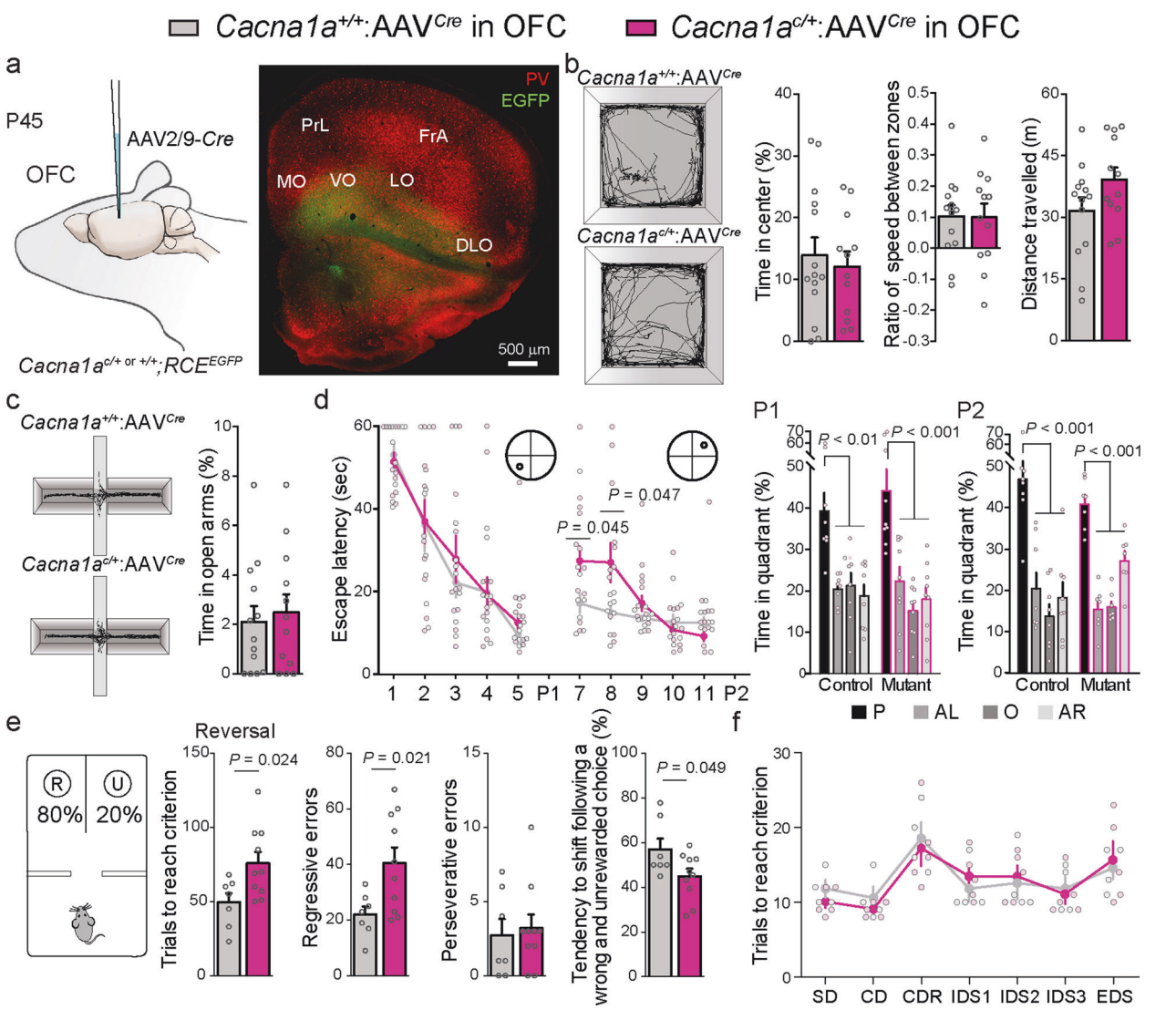

Fig. 5 Cognitive rigidity recapitulated by a targeted heterozygous deletion of *Cacna1a* in the OFC. a The OFC of *Cacna1a*$^{c/+}$;*RCE*^{EGFP} mutant and *Cacna1a*$^{+/+}$;*RCE*^{EGFP} control mice were injected with an AAV2/9-Cre expressing virus. The infection was mostly restricted to the OFC as shown by infected cells expressing EGFP. **b** Open field: an illustrative example of a travel path from a control (top) and OFC-Cre-injected *Cacna1a*$^{c/+}$ mutant (bottom). Mean time spent in the central zone of the Open field (left) ($n = 14$ controls, $n = 12$ OFC-Cre-injected *Cacna1a*$^{c/+}$), ratio of the speed in the centre zone compared to the periphery (middle) ($n = 14$ controls, $n = 12$ mutants) and total distance travelled (right) ($n = 13$ controls, $n = 12$ mutants). **c** Elevated Plus Maze: representative paths taken by a control (top) and an OFC-Cre-injected *Cacna1a*$^{c/+}$ mutant (bottom) in the Elevated Plus Maze, with time spent on the open arms of the maze ($n = 14$ controls, $n = 12$ mutants). **d** Morris Water Maze: learning curve in the Morris Water Maze task (left), with reversal on day 7 (inserts depict the localisation of the platform). Probe test (right): probe tests were conducted on days 6 and 12 (P: platform; AL: adjacent left; O: opposite; AR: adjacent right; P1: probe test 1; P2: probe test 2) ($n = 9$ controls, $n = 13$ mutants). **e** Probabilistic reversal learning task: diagram of the maze (left) showing a reward-containing well (R) and an unrewarded empty well (U). Number of trials needed to reach criterion in the reversal step, the number of regressive errors (second graph) the number of perseverative errors (third graph) and the shifting behaviour (fourth graph) ($n = 7$ controls, $n = 10$ mutants). **f** Attention set shifting task: number of trials needed to reach criterion in the different steps of the task (SD: simple discrimination; CD: compound discrimination; CDR: compound discrimination (reversal); IDS1-3: intra-dimensional shift 1 to 3; EDS: extra-dimensional shift) ($n = 4$ controls, $n = 5$ mutants). Error bars represent mean ± s.e.m. Two-tailed Student's *t* test was applied for *P* values in **b**, **c**, **d** (day 7 and 8) and **e**. Two-way ANOVA repeated measure with Bonferroni's t-test was applied to **d**. Two-way ANOVA with Bonferroni's t-test was conducted in **d** (probe test) and **f**.

characterized the effect of the chemogenetic activation on layer V PV-INs excitability with whole-cell recordings in mPFC slices obtained from *PV*^{Cre};*Cacna1a*$^{c/+}$ mice 2 weeks after injection. Bath application of CNO indeed resulted in membrane depolarization, increased membrane resistance and firing rates (Fig. 6b–h) in PV-INs of mice expressing the hM3Dq, confirming the activation of these cells. By contrast, CNO had no effect on PV-INs of mice expressing the 246-pAAV-hSYN-DIO-mCherry control virus.

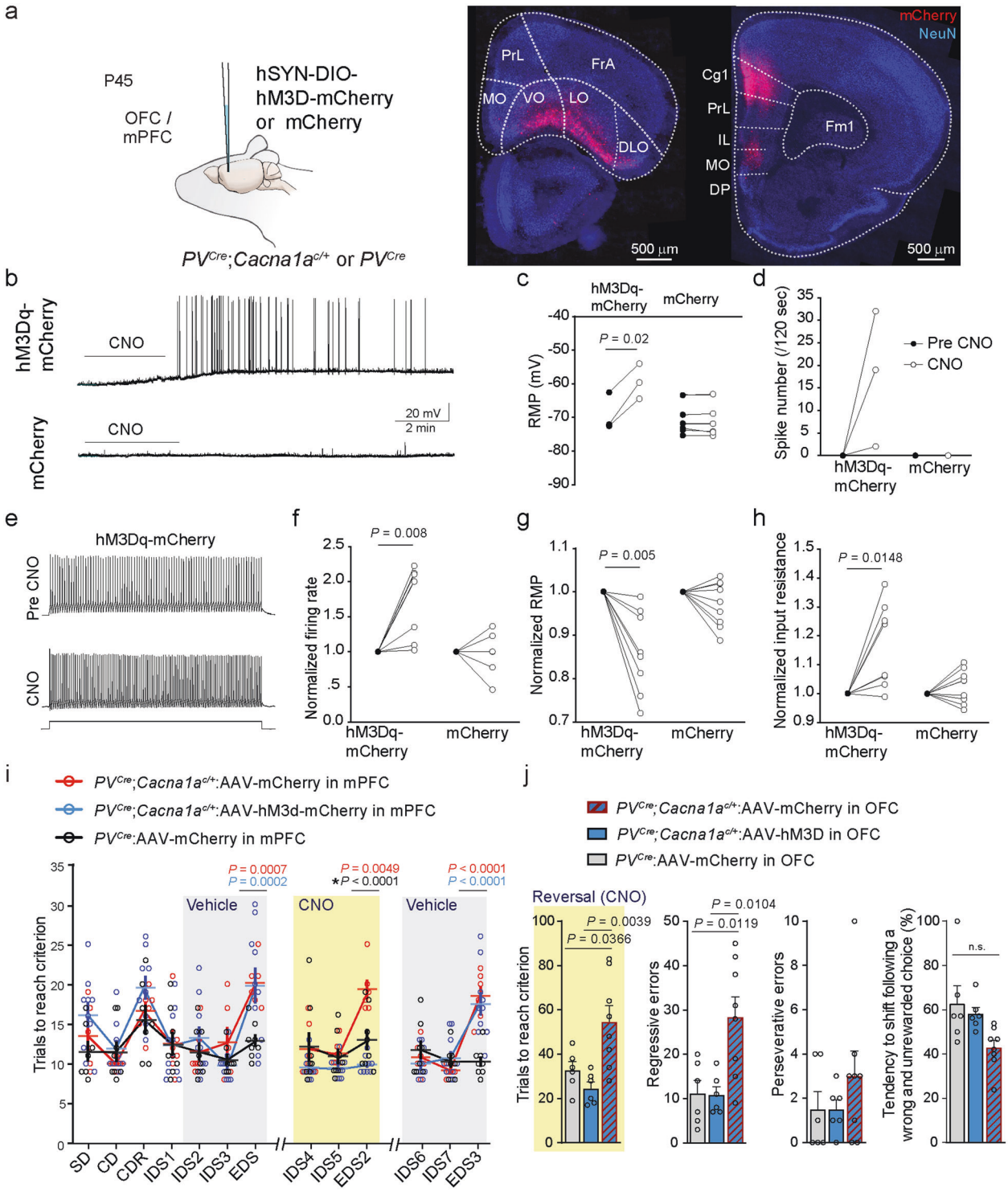

We next tested the therapeutic benefit of a chemogenetic activation of mPFC PV-INs on selective attention in P60 PV^{Cre};$Cacna1a^{c/+}$ mice tested 2 weeks after bilateral injections of 246-pAAV-hSYN-DIO-hM3D (Gq)-mCherry viruses. These mice were compared to littermate PV^{Cre} control mice and PV^{Cre};$Cacna1a^{c/+}$ mutants, both injected with a control AAV2/9-FLEX-mCherry virus to account for the potential impact of CNO on behaviour in the absence of the hM3D(Gq) receptor. All mice were evaluated in an extended Attention Set Shifting Task (Supplementary Fig. 3b) where two IDS tasks and an EDS task were repeated

◀ **Fig. 6 The chemogenetic activation of PV-INs in the mPFC or OFC respectively rescues the selective attention deficits and the reversal learning deficits in PV^{Cre};$Cacna1a^{c/+}$ mutants. a** PV^{Cre};$Cacna1a^{c/+}$ mutant or PV^{Cre} control mice were injected in the OFC or the mPFC with Cre-dependent AAV2/9- hSYN-DIO-hM3D-mCherry or AAV2/9-hSYN-DIO-mCherry control virus. The infection was restricted to the OFC or mPFC as shown by infected cells expressing mCherry. Representative traces (**b**) and summary graphs (**c**, **d**) showing the effects of short bath application of CNO (1 µM) on L5 PV-INs in mPFC slices from PV^{Cre};$Cacna1a^{c/+}$ mice injected with AAV-hM3Dq-mCherry ($n = 3$ cells/1 mice) and AAV-mCherry ($n = 7$ cells/2 mice). CNO depolarized the resting membrane potential (RMP) and induced firing in mice injected with the hM3Dq-mCherry virus. Representative traces (**e**) and summary graphs showing CNO effects on (**f**) depolarization-evoked firing normalized to baseline (Pre CNO; 240 pA current injection), (**g**) RMP normalized to baseline, and (**h**) input resistance normalized to baseline, in PV-INs from mPFC of AAV-hM3Dq-mCherry-injected ($n = 8$ cells/3 mice) and AAV-mCherry-injected ($n = 8$ cells/3 mice) PV^{Cre};$Cacna1a^{c/+}$ mice. **i** Modified Attention set shifting task: number of trials needed to reach criterion in the different steps of the task (SD: simple discrimination; CD: compound discrimination; CDR: compound discrimination (reversal); IDS1-7: intra-dimensional shift 1 to 7; EDS1-3: extra-dimensional shift 1 to 3). Yellow shading represents CNO injections ($n = 7$ mPFC-mCherry-injected controls; 8 mPFC-hM3Dq-injected mutants; 6 mPFC-mCherry-injected mutants). Values for mutants are compared to those from controls (red: AAV-mCherry injected mutants, blue: AAV-hM3d-mCherry injected mutants). With CNO injections, AAV-hM3d-mCherry injected mutants behave as controls. (*) mPFC-mCherry-injected PV^{Cre};$Cacna1a^{c/+}$ mutants are compared to mPFC-hM3Dq-injected PV^{Cre};$Cacna1a^{c/+}$ mutants. **j** Probabilistic reversal learning task: number of trials needed to reach criterion in the reversal step (first graph), the number of regressive errors (second graph), the number of perseverative errors (third graph) and the shifting behaviour after an incorrect unrewarded choice (fourth graph) ($n = 6$ OFC-mCherry-injected PV^{Cre} controls; $n = 6$ OFC-hM3Dq-injected PV^{Cre};$Cacna1a^{c/+}$; $n = 8$ OFC-mCherry-injected PV^{Cre};$Cacna1a^{c/+}$). Error bars represent mean ± s.e.m. Two-tailed Student's *t* test was applied in **c**, **d**, **f**, **g**, **h**. Wilcoxon Rank test was applied for values in e, followed by a two-way repeated measure ANOVA with a Bonferroni's post-hoc correction. Two-way unrepeated measure ANOVA with a Bonferroni's post-hoc correction, was applied to **i** and **j**. Also, One-way unrepeated measure ANOVA, with a Bonferroni's post-hoc correction, was applied in the analysis of errors and shifting behaviour in **j**).

twice after the initial Attention Set Shifting Task (day 1: training; day 2: IDS1, IDS2, IDS3, ESD1; day 3: IDS4, IDS5 and EDS2; day 4: IDS6, IDS7 and EDS3). On days 2 and 4, mice were injected with vehicle 30 min prior to the experiment. On day 3, PV-INs were activated with a single injection of CNO (3 mg/kg) 30 min prior to the experiment. As expected, mutants injected with either virus (PV^{Cre};$Cacna1a^{c/+}$;AAV-mCherry and PV^{Cre};$Cacna1a^{c/+}$;AAV-hM3d) displayed attention set-shifting deficits compared to injected PV^{Cre} controls (PV^{Cre}; AAV-mCherry), with clear deficits in the EDS1 task (Fig. 6i). Interestingly, the chemogenetic activation of PV-INs in the mPFC of PV^{Cre};$Cacna1a^{c/+}$ mutants receiving a single CNO injection on day 3 corrected the selective attention deficit in PV^{Cre};$Cacna1a^{c/+}$ mutants injected with the AAV-hM3d virus but not of PV^{Cre};$Cacna1a^{c/+}$ mutants injected with the control AAV-mCherry virus (Fig. 6i). This rescue was not an effect of habituation and also did not last in time as the behavioural deficit returned on day 4. Importantly, PV^{Cre};$Cacna1a^{c/+}$ mice expressing the control AAV-mCherry virus displayed attention deficits on each 3 EDS tests when compared to controls, despite CNO treatment, suggesting that the behavioural improvement was not due to an off-target effect of converted CNO to clozapine or N-desmethylclozapine (NDMC) (Fig. 6i) [37].

The Targeted chemogenetic activation of OFC PV-INs restores cognitive flexibility in PV^{Cre};$Cacna1a^{c/+}$ mutants

To explore the therapeutic benefit of a chemogenetic activation of OFC PV-INs on cognitive flexibility, we selectively activated PV-INs in the OFC of P60 PV^{Cre};$Cacna1a^{c/+}$ mutants 2 weeks after bilateral injections of 246-pAAV-hSYN-DIO-hM3D(Gq)-mCherry in the OFC. These mutants were compared to PV^{cre} and PV^{Cre};$Cacna1a^{c/+}$ littermate injected with a control AAV-mCherry virus. Interestingly, CNO (3 mg/kg) enhanced the cognitive flexibility of mutant mice expressing the hM3D(Gq) compared to mutant mice expressing only the control mCherry virus (Fig. 6j). This level of flexibility was similar to the level observed in the mCherry injected control mice. Indeed, compared to mCherry expressing mutant mice, hM3D(Gq) expressing mutant mice required less trials to reach criterion on the reversal task, and they made significantly less regressive errors.

Taken together, our results suggest that the attention deficits and reversal learning deficits associated with *Cacna1a* haploinsufficiency in PV^{Cre};$Cacna1a^{c/+}$ mice can be rescued by selectively enhancing the activity of PV-INs in the mPFC and OFC respectively.

Discussion

This study reveals the extensive neuropsychological deficits associated with *CACNA1A* LOF mutations in humans, including inattention and cognitive rigidity. Mechanistically, we found that *Cacna1a* haploinsufficiency selectively impairs GABA release from cortical PV-INs while preserving glutamate release from PCs. Further, we demonstrate that a selective deletion of *Cacna1a* in the mPFC impairs selective attention while a targeted deletion in the OFC is sufficient to induce cognitive rigidity. Importantly, we show that both deficits can be rescued by a targeted activation of PV-INs in these specific frontal regions in PV^{Cre};$Cacna1a^{c/+}$ mice. Thus, our findings reveal the critical contribution of disrupted frontal cortical inhibition to the cognitive and behavioural deficits associated

with *CACNA1A* haploinsufficiency and may ultimately help tailor new therapies to improve cognition and behaviour in patients with *CACNA1A*-associated disorders.

Neurocognitive deficits associated with *CACNA1A* mutations have been reported in patients with FHM1, spinocerebellar ataxia type 6 (SCA6), and in some cases of EA2, as reviewed elsewhere [38]. Further, *de novo CACNA1A* missense mutations have recently been recognized as an important cause of epileptic encephalopathies with profound intellectual disability [3, 6, 39]. In the current paper, we provide in-depth characterization of the neuropsychological profile associated with *CACNA1A* LOF mutations, revealing pronounced deficits in selective attention, cognitive rigidity (in a sub-set of patients with ASD), together with deficits in working and episodic memory. These previously overlooked neurocognitive deficits significantly impacted the patients live trajectories: most patients required special education, often failing to obtain high school degrees or to hold independent employment [2]. Thus, the identification of *CACNA1A* LOF mutations should prompt clinicians to assess the patients' neuropsychological profile and to provide early guidance and psychostimulants to improve long-term outcome.

Modelling in mice has provided insights in the cellular basis underlying some aspects of the cognitive behavioural deficits associated with *CACNA1A* LOF mutations. *Cacna1a* knockout mice develop absence seizures, dystonia and ataxia in the homozygous state [40, 41], preventing the evaluation of their behavioural and cognitive skills; while heterozygous mice were initially described as asymptomatic [41]. However, detailed behavioural analysis of heterozygous leaner mice ($Tg^{la/+}$) revealed spatial learning deficits at 6 months, a progressive decline in spatial memory at 20 months and of motor skills at 6–12 months [42]. Similarly, rolling Nagoya$^{+/-}$ mutant mice that behave normally at 2 months of age display a progressive decline in motor performance and memory at 22 months of age [43, 44]. Such progressive cognitive decline is reminiscent of what we observed in adult patients with *CACNA1A* LOF mutations [2], and what was described in aging patients with *CACNA1A*-asociated SCA6 [45]. Further, conditional NEX^{Cre};$Cacna1a^{c/+}$ mutant mice, carrying a targeted deletion in telencephalic excitatory neurons, sparing the cerebellum and INs, display mild spatial memory impairments [31] suggesting that other cell types likely contribute to the cognitive-behavioural deficits observed in constitutive knockout mice. Indeed, in the current study, we demonstrate that disinhibition of frontal cortical circuits, resulting from the selective heterozygous deletion of *Cacna1a* in PV-positive populations of the OFC and mPFC, induces cognitive rigidity and selective attention deficits, two major features of the neurocognitive disabilities observed in patients with heterozygous *CACNA1A* LOF mutations, suggesting a major contribution of altered IN function to the overall neurobehavioural phenotype.

Dysfunction of PV-INs and disruption of cortical inhibition have been postulated to contribute to neurodevelopmental or psychiatric disorders, including epilepsy, autism and schizophrenia [46–48]. Indeed, various models of neurodevelopmental disorders presenting altered specification, migration, maturation or function of cortical PV-INs have been described to date [46, 47]. For instance, mutations in the *SCN1A* gene, encoding the α1 subunit of $Na_V1.1$ sodium channels, cause Dravet syndrome (OMIM #607208) that is characterized by severe refractory epilepsy and ID. *Scn1a* LOF mutations reduce the excitability of INs, particularly of PV-INs [49, 50]. Heterozygous *Scn1a* LOF mutations impairs inhibitory transmission and causes a variety of cognitive-behavioural deficits including hyperactivity, stereotypies, social interaction deficits and impaired context-dependent spatial memory [51]. This phenotype can be recapitulated by a targeted *Scn1a* deletion in forebrain GABAergic INs and can be rescued with low-dose benzodiazepines, stressing the importance of INs dysfunctions in the cognitive-behavioural co-morbidities of Dravet syndrome [51]. Further, the conditional deletion of *Scn1a* in forebrain INs ($Dlx1/2^{Cre}$;$Scn1a^{fl/+}$) [52] or in PV-positive neuronal populations ($Ppp1r2^{Cre}$;$Scn1a^{fl/+}$) [49] results in epilepsy and early lethality. In a similar fashion, LOF mutations of the *MECP2* gene cause Rett syndrome in girls (OMIM #312750), characterized by progressive microcephaly, developmental regression, autistic-like features and epilepsy. A targeted deletion of *MecP2* in GABAergic neurons ($Viaat\text{-}Mecp2^{-/y}$) or in forebrain INs ($Dlx6^{Cre}\text{-}Mecp2^{-/y}$) in mice reduces GABA release from cortical INs and impairs hippocampal LTP, resulting in autistic-like behaviours, including repetitive and compulsive behaviours, stereotypies and altered social behaviours, as in knock-out mice [53]. Furthermore, two schizophrenia susceptibility genes, *NRG1* (encoding neuregulin-1) and *ERBB4* (encoding NRG1's receptor), are critical for PV-INs development [54], excitability [55], connectivity [56] and function [57–60]. Mice with targeted deletion of *ErbB4* in PV-INs (PV^{Cre};$Erbb4^{fl/fl}$) display a variety of cognitive behavioural impairments (hyperactivity, impaired working memory, deficits in pre-pulse inhibition and socialization) [59, 60] and are more susceptible to pharmacologically [55] and kindling-induced [61] seizures. Thus, our data further shows that an imbalance between cortical excitation and inhibition, through synaptic impairment of PV-INs, suffices to induce cognitive-behavioural deficits, as observed in a range of genetic neurodevelopmental disorders [62, 63].

Our findings are particularly critical in illustrating the consequences of cortical disinhibition within particular neuronal circuits and support previous suggestions that fontal cortical PV-INs are essential for selective attention

and cognitive flexibility. Indeed, *uPAR*$^{-/-}$ mice, deficient for the urokinase plasminogen activator receptor (uPAR), the mouse ortholog of the autism-susceptibility *PLAUR* gene, show significant reductions of PV-INs in the parietal and anterior cingulate cortex and exhibit autistic-like behaviours, increased anxiety, altered socialization and an increased susceptibility to PTZ-induced seizures [64, 65]. In addition, *uPAR*$^{-/-}$ mice show selective impairment in attention set-shifting and in extinction of cued-fear conditioning, suggesting selective deficits in mPFC circuits [36], as well as impairment in reversal learning, suggesting alterations in OFC circuits [21]. Similarly, offspring of mothers with maternal immune activation (MIA) display reduced numbers of mPFC PV-INs, reduced cortical inhibition and attention set shifting deficits [23]. Further, a targeted ablation of PV-INs in the oFC (AAV-FLEX-TeLC injected in *PV*^{cre} mice) reduces working memory and cognitive flexibility in mice [25]. Thus, PV-INs in frontal circuits are required to achieve selective attention and cognitive flexibility and their perturbation in specific genetic context, such as *CACNA1A* haploinsufficiency, is sufficient to induce significant behavioural phenotypes.

The mechanism by which disruption of PV-INs mediated inhibition results in such dramatic behavioural phenotypes is not fully understood, but it likely reflects the roles of these cells in constraining local excitability while regulating neuronal network oscillations through local and long-range inhibition. Indeed, PV-INs regulate PCs spike timing through fast, stable and precise perisomatic inhibition of target PCs, resulting in robust feed-forward inhibition [66]. Further, PV-INs contribute to the regulation of network activities by generating gamma network oscillations that determine time windows for PCs activation, regulating the timely activation of neuronal assemblies [17, 67, 68]. Gamma oscillations are critical for adequate cortical processing [15, 17, 68], attention and memory [69]. Further, the coupling of gamma oscillations with theta rhythms appears critical for neuronal coding and contributes to cognitive functions, such as episodic memory [70]. Interestingly, *Cacna1a* null mice present reduced cortical gamma oscillations [71], likely reflecting deficits in PV-INs function. In the mPFC, PV-INs are critical for selective [16, 20, 36] and sustained attention [19]. Successful attention allocation during an attention set-shifting task synchronizes mPFC PV-INs, enhances gamma oscillations and phase-locks the firing of PCs and their modulation by gamma oscillations [19]. Interestingly, the optogenetic inhibition of PV-INs in wild-type mice decreases performance in the three-choice serial reaction time task, a task designed to assess sustained attention. On the other hand, the activation of these cells re-established performance [19], underlying the importance of PV-INs in maintaining attention. In line with these publications, our data strongly suggests that a dysfunction of PV-INs in the mPFC and OFC induces selective attention deficits and cognitive rigidity respectively, and that these deficits can be rectified by targeted therapies to selectively activate PV-INs, thus re-establishing proper regulation of cortical network oscillations. Ultimately, our findings may have therapeutic implications for patients with genetic disorders impairing PV-IN function as targeted IN stimulation is gaining momentum in translational studies and are being optimized for use in humans [72].

Online methods

Neuropsychological evaluation of patients with *CACNA1A* LOF mutations

We previously described a cohort of 16 patients with *CACNA1A* LOF mutations [2]. All six affected children from this cohort were investigated here using standardized neuropsychological tools, including the Weschler Intelligence Scale for Children–4th edition (WISC-IV) [73, 74] and the Conners 3rd edition (parent and teacher forms) [75]. Further testing was conducted in 4 patients without severe ID or severe ASD using the following tools: the Delis-Keplan Executive Function System (Subtests: Colour-Word Interference, Verbal Fluency and Design Fluency) [76], the Tower of London dx-Child [77], the Test of Everyday Attention for Children [78] (subtests: Score!, and Map Mission), the Child Memory Scale (subtest: Stories) [79], the Rey–Osterrieth Complex Figure Test, the Beery-Buktenica Developmental Test of Visual-Motor Integration [80], the Purdue Pegboard Test [81] and the Expressive One Word Picture Vocabulary Test [82]. Results are reported in Fig. 1 as mean Z scores to age-matched population data. The significance was established using cut-off values of $Z <= -1.5$ for cognitive tests (Fig. 1a, c) and $Z <= -2.0$ for behavioural scales (Fig. 1b). All participants were tested in French.

Animals

All animal rearing, handling and experimentation were done in accordance with the CCAC ethical guidelines, as approved by the CHU Ste-Justine Animal Ethics Board (protocols # 671 for rearing and handling, and # 598 for experimentation). *PV*^{Cre};*Cacna1a*$^{c/+}$ mutant mice carrying a targeted *Cacna1a* intragenic deletion in PV-positive neuronal populations were generated by breeding *PV*^{Cre} mice [83] (S. Arber, Basel U., Switzerland) with the *Cacna1a*$^{c/c}$ mice (A. van den Maagdenberg, U. Leiden, Leiden, Netherlands), in which exon 4 of the *Cacna1a* gene is flanked by two loxP sites, leading to an effective loss-of-function of the

gene, as demonstrated previously [31, 84]. Similarly, *Emx1*^{Cre};*Cacna1a*$^{c/+}$ mice, carrying a targeted deletion of the *Cacna1a* gene in all cortical PCs, were generated using the *Emx1*^{Cre} knock-in line [32] (S. Itohara, Brain Science Institute, Riken U., Japan). *PV*^{Cre};*Cacna1a*$^{c/+}$ and *Emx1*^{Cre};*Cacna1a*$^{c/+}$ mice were compared to control littermate devoid of Cre expression. Mice carrying a targeted heterozygous *Cacna1a* deletion in specific frontal cortical regions, including the orbitofrontal cortex (*Cacna1a*$^{c/+}$;*RCE*$^{EGFP/+}$: AAV-Cre injected in oFC) or medial prefrontal cortex (*Cacna1a*$^{c/+}$;*RCE*$^{EGFP/+}$: AAV-Cre injected in mPFC), were generated by injecting Cre-expressing AAVs (Penn Vector Core) in *Cacna1a*$^{c/+}$ mice. *Cacna1a*$^{+/+}$: AAV-Cre injected littermate were used as control. The Cre-reporter allele *RCE*^{EGFP} (G. Fishell, NYU, USA) [85] was used to track recombination. Injections were performed at 6 weeks of age and behavioural experiments were performed in 2–3 months old animals. For all experiments, mutant mice were compared with sex-matched littermate controls and investigators were blind to the genotype.

Viral injections

Different viruses were used for different experimental paradigm. To generate mutant mice carrying focal *Cacna1a* deletions, we injected a Cre-expressing virus (AAV2/9.CMV.PI.Cre.rBG, Penn Vector Core) in *Cacna1a*$^{c/+}$;*RCE*^{EGFP} mice. To test synaptic release from populations of PV-IN in specific frontal areas using optogenetics, we injected a Cre-dependent ChR2-expressing virus (AAV9.CAGGS.Flex.ChR2-tdTomato.WPRE.SV40) or a control Cre-dependent tdTomato virus (AAV9.CAGGS.Flex.tdTomato. WPRE.bGH), both from Penn Vector Core, in *PV*^{Cre};*Cacna1a*$^{c/+}$;*RCE*^{EGFP} mice. Finally, to test the therapeutic benefit of a targeted chemogenetic activation of PV-INs in specific frontal networks, we injected the Cre-dependent 246-pAAV-hSYN-DIO-hM3D(Gq)-mCherry virus (CHUL virus core, CIUSSS de la Capitale-Nationale), or a control AAV9.CAG.Flex.tdTomato.WPRE.bGH virus in *PV*^{Cre};*Cacna1a*$^{c/+}$;*RCE*^{EGFP} mutant mice or *PV*^{Cre};*Cacna1a*$^{+/+}$;*RCE*^{EGFP} controls.

Injections were conducted under sterile conditions and with general anesthesia. Animals were mounted on a stereotaxic apparatus and anaesthetized with isofluorane. Following small bilateral craniotomies, the viruses were injected in the orbitofrontal cortex (AP: 2.6; ML: ± 1; DV: −2 to bregma) or in the medial prefrontal cortex (AP: 1.8; ML: ± 0.3; DV: −1.75 to bregma). 0.4 µl of virus solution was injected bilaterally with a glass pipette using Nanoject II injector (Drummond). The injections were made at P45-60, 2 weeks prior to the behavioural or electrophysiological experiments.

Electrophysiology

Optogenetic activation of PV-INs

Acute brain slices were prepared as described previously [11] from *PV*^{Cre};*Cacna1a*$^{c/+}$ mutant or *PV*^{Cre} control mice injected with AAV9.CAGGS.Flex.ChR2-tdTomato.WPRE.SV40 in the mPFC or oFC. Briefly, animals (8–10 weeks old) were anesthetized and the brain was placed in a cold N-methyl-D-glucamine (NMDG)-based cutting solution containing (in mM) 92 NMDG, 2.5 KCl, 1.25 NaH_2PO_4, 30 $NaHCO_3$, 20 HEPES, 25 glucose, 2 thiourea, 5 Na-ascorbate, 3 Na-pyruvate, 0.5 $CaCl_2$ and 10 $MgSO_4$. Coronal cortical slices (300 µm thick) were cut on a vibratome (Model VT1000S; Leica, Germany), incubated in NMDG-based cutting solution for 12 min at 32 °C. Slices were then placed in HEPES-based artificial cerebrospinal fluid (ACSF) containing (in mM) 92 NaCl, 2.5 KCl, 1.25 NaH_2PO_4, 30 $NaHCO_3$, 20 HEPES, 25 glucose, 2 thiourea, 5 Na-ascorbate, 3 Na-pyruvate, 2 $CaCl_2$ and 2 $MgSO_4$, at room temperature for at least 60 min. For recordings, slices were transferred to a submersion chamber mounted on an upright microscope (Zeiss Axioskop; Carl Zeiss, Oberkochen, Germany) equipped with a long-range water-immersion objective (40x; Modulation Optics, Greenvale, NY), DIC optics, epifluorescence and CCD camera. Whole-cell voltage-clamp recordings were obtained under visual guidance from PCs in layer V using intracellular solution containing (in mM) 130 CsCl, 0.5 EGTA, 2 $MgCl_2$, 10 HEPES, 2 Mg-ATP, 0.4 Tris-GTP, 5 phosphocreatine and 5 QX-314 (pH 7.3 with CsOH) and ACSF containing (in mM) 125 NaCl, 2.5 KCl, 1.25 NaH_2PO_4, 1 $MgCl_2$, 2 $CaCl_2$, 25 $NaHCO_3$, and 25 glucose. Signals were sampled using Multiclamp 700 A amplifiers (Molecular Devices, USA), low-pass filtered at 5 or 2 KHz, digitized at 20 KHz with Digidata 1440 A and pClamp 10.0 (Molecular Devices, USA), and analyzed off-line with the Clampfit software (Molecular Devices, USA). Inhibitory post-synaptic currents (IPSCs) were evoked at a holding potential of –70 mV, in the presence of 10 µM CNQX, 50 µM DL-APV. ChR2 was activated via an optic fiber (1-mm diameter; Edmunds Optic) coupled to a 470-nm custom-made LED system positioned above the slice, as described previously [86]. The measured LED power was 25–26 mW at the end of the light guide. To determine input–output function of light-evoked IPSCs, series of light flashes of different duration (0.2–5 ms) were given at 30 s intervals and a single cell was recorded per slice. The IPSCs were completely blocked by the $GABA_A$ receptor antagonist GABAzine, confirming they were $GABA_A$-receptor mediated.

Given the inherent variability in optogenetic experiments due to small differences in injection site, viral transduction

and ChR2 expression levels, the following series of precautions were taken to minimize optogenetic response variability. Only slices showing similar strong tdTomato expression were included in the study, and specificity and efficacy of virus transduction were verified for each animal with fluorescence microscopy. For each series of experiments (genotype control vs conditional mutant), virus injections and slice experiments were interleaved with control and mutant animals, with the experimenter blind to genotype until after data analysis.

Paired recordings

Acute slices from mPFC were obtained as described above from PV^{Cre};$Cacna1a^{c/+}$;RCE^{EGFP} and PV^{Cre};RCE^{EGFP} mice. Paired whole-cell recordings were obtained from layer V fluorescently labelled PV-INs in current-clamp mode and PCs in voltage-clamp mode. Current-clamp intracellular solution contained (in mM) 120 $KMeSO_3$, 0.5 EGTA, 10 KCl, 10 HEPES, 4 Mg-ATP, 0.3 Tris-GTP, 10 phosphocreatine and 0.1% biocytin (pH 7.3 with KOH). Voltage-clamp intracellular solution contained (in mM) 130 $CsMeSO_3$, 0.2 EGTA, 8 CsCl, 1 $MgCl_2$, 10 HEPES, 3 Mg-ATP, 0.6 Tris-GTP, 10 phosphocreatine and 0.1% biocytin (pH 7.3 with CsOH). Extracellular recording solution contained (in mM) 124 NaCl, 2.5 KCl, 1.25 NaH_2PO_4, 2 $MgSO_4$, 2 $CaCl_2$, 25 $NaHCO_3$, and 12.5 glucose. Single action potentials were induced in presynaptic PV-INs by brief depolarizing current pulses (2 ms; 0.1 Hz), and unitary IPSCs were recorded in PC at a membrane potential of 0 mV. IPSCs were blocked by GABAzine (10 µM) and thus $GABA_A$ receptor-mediated. Short-term plasticity of IPSCs was assessed with paired-pulse stimulations (inter-pulse interval 50 ms, 0.1 Hz).

Evoked EPSCs in $Emx1^{Cre}$;Cacna1a$^{c/+}$ mutants

Acute slices from OFC were obtained as described above from $Emx1^{Cre}$;$Cacna1a^{c/+}$ and $Emx1^{Cre}$;$Cacna1a^{+/+}$ mice. Whole-cell voltage clamp recordings were obtained from layer V PCs with an intracellular solution containing (in mM) 130 $CsMeSO_3$, 0.2 EGTA, 8 CsCl, 1 $MgCl_2$, 10 HEPES, 3 Mg-ATP, 0.6 Tris-GTP, 10 phosphocreatine and 0.1% biocytin (pH 7.3 with CsOH). The ACSF contained (in mM) 125 NaCl, 2.5 KCl, 1.25 NaH_2PO_4, 1 $MgCl_2$, $CaCl_2$ 2, 25 $NaHCO_3$, 25 glucose and 0.01 GABAzine. Excitatory postsynaptic currents (EPSCs) were evoked by electrical stimulation (pulses 80–280 µA, 0.05 ms duration, 0.1 Hz frequency) with a concentric bipolar stimulating electrode (FHC) placed ~250 µm from the soma.

PV-IN recordings and CNO effects in slices

Acute slices from mPFC were obtained as described above from PV^{Cre};$Cacna1a^{c/+}$ mice injected with 246-pAAV-hSYN-DIO-hM3D(Gq)-mCherry or AAV9.CAG.Flex.tdTomato.WPRE.bGH viruses in the mPFC. Whole-cell current clamp recordings were obtained from fluorescently labelled layer V PV-INs. The intracellular and extracellular solutions were as described for paired recordings. Effects of bath application of CNO (1 µM) were assessed on resting membrane potential, input resistance (measured from the slope of I-V relation obtained from −120 to 40 pA current pulses), spontaneous action potential firing, and firing rate evoked by long (500 ms) depolarizing current pulses.

Behaviour

All behavioural experiments were conducted in aged-matched mutants and littermate controls between P60-P90, at a similar daytime period, by investigators blinded to the genotype and viruses used. The animals were placed in the experimental room 30 min before testing. All assays were conducted under video-tracking (Logitech c615 camera, SMART tracking system, Harvard Apparatus), except the Reversal learning task and Attention set-shifting task that were quantified manually.

The behavioural tasks were conducted sequentially from P60 onwards: Openfield (P60), Elevated Plus Maze (P62), Morris Water Maze (P64), Attention set-shifting or probabilistic reversal learning tasks (P80). Separate sets of mice underwent the Object Recognition and Three Chamber Maze assays.

Openfield

The open field consists of a square of 45×45 cm surrounded by a 45 cm wall, illuminated with dim light. Mice were placed in the centre of the maze and their behaviour was recorded for 10 min. Time spent in the central area of the field (45% of the total surface), covered distance and pace difference between central and peripheral zones were measured. The speed ratio were defined as $\text{Speed}_{\text{ratio}} = [(P_C - P_S)/(P_C + P_S)]$ where P is the average pace in C, the centre, and S, the sides of the maze. The open-field arena was cleaned with ethanol 70% between each trial.

Elevated plus maze

The Elevated Plus Maze comprises two closed arms surrounded by 20 cm high walls and two open arms. Each mouse was placed in the centre (5 × 5 cm) of the maze

facing one of the closed arms, and their behaviour was recorded for 5 min. Total distance, speed, number of entries and time spent in the open arms, closed arms and central zone were quantified post-hoc. The maze was cleaned with 70% ethanol between each trial.

Morris water maze

The Morris Water Maze consisted of a circular tank of 120 cm of diameter filled with opaque water stained with non-toxic white paint (Brault & Bouthillier). Water was held at room temperature (21 ± 1 °C). *Initial acquisition task*. The mice were placed in the pool and were expected to locate a submerged escape platform using the visible cues present in the room. Spatial learning was assessed over 5 days, with 4 trials per day. During each trial, mice were allowed to swim until they found the platform where they remained for 15 s before being dried and returned to their cage. Mice that failed to find the platform in less than 60 s trials were guided to the platform where they remained for 10 s. The time required to find the platform was recorded and averaged across the sessions performed daily. *Probe test*. Spatial memory was determined during a probe test on the 6th day, after removing the platform. The time spent in each quadrant was assessed over a 60 s. period. *Reversal task*. On day 7, the platform was submerged in the opposite quadrant compared to the first 5 days, and spatial learning (time to reach the platform) was assessed daily as above. A second probe test was done on the 12th day (as above). This was followed by a cue trial in which the platform was visible, thus documenting proper visual perception. Mice that took more than 60 s. to reach the visible platform were retrospectively excluded from the experiment.

Object recognition task

The object recognition task was conducted in the Openfield apparatus. Mice were first placed 5 min in the empty arena and allowed to freely explore the arena. Their behaviour was then recorded over the following 10 min period, in the same arena but in the presence of two similar objects (2 cm squared dices). Following this trial, mice were removed for 5 min, then placed again for 10 min in the same arena in which one of the dice was displaced to the opposite corner. Following this trial, mice were removed for 5 min, and then placed again for 10 min in the same arena in which the unmoved dice was replaced by a pyramid on which was fixed a syringe filter. The mice's behaviour was recorded and the time spent interacting with each object was quantified. Animals were scored as interacting with the objects when their nose was in contact with the object, or pointing toward the object within a defined distance (1.5 cm). Standing, sitting or leaning at/on the objects was not scored as object interaction. The discrimination index was defined as $D_{index} = [(T_A - T_B)/(T_A + T_B)]$ where T is the interaction time with the object, A is the displaced or changed object and B is the unmoved or unchanged object. At the end of the whole experiment, the maze and objects were cleaned with 70% ethanol.

Three chamber maze

The three-chamber maze was composed of a rectangular arena (70 ×45 cm) surrounded by 30 cm tall transparent walls and separated in three equally sized zones by two 45×30 cm transparent walls. The dividing walls had a door allowing the mice to circulate between zones. The animal were first placed in the middle of the central chamber and allowed to explore all empty chambers for 5 min. After habituation, an unfamiliar mouse of the same sex and age (Stranger 1 (S1)) was placed inside a small wire cage and an empty cage was added in the opposite zone. The middle zone remained empty. The tested animal was allowed to freely explore the three chambers of the apparatus for 10 min. At the end of this 10 min, a new unfamiliar mouse of the same sex and age (Stranger 2 (S2)) was placed in the previously unoccupied wire cage and the tested mouse was observed for an additional 10 min to assess preference for social novelty. S1 and S2 animals originated from different home cages and had never been in physical contact with the tested mice or between each other. The sociability was evaluated by quantifying the time spent by the tested mice in each chamber during the second 10 min session whereas the social novelty was evaluated by quantifying the time spent by the tested mice in each chamber during the last session. The discrimination index was defined as $D_{index} = [(T_A - T_B)/(T_A + T_B)]$ where T is the interaction time, A is the S1 for sociability and S2 for social novelty part of the task and B is the Object for sociability and S1 for social novelty. The maze and cages were cleaned with 70% ethanol at the end of the task.

Attention set-shifting task

PV^{Cre}; $Cacna1a^{c/+}$ and mPFC-Cre-injected $Cacna1a^{c/+}$ mice were tested on the attention set-shifting task, described by Heisler [29]. This experiment was performed in a home-made acrylic rectangular-shaped maze (30 cm long × 20 cm wide × 18 cm high) divided in half by a guillotine-like door that extended the width of the maze. One half served as the start area and the other half served as the choice area. In the choice area, an acrylic wall (12 cm long × 18 cm high) presenting four ¼" diameter sniffing holes on the bottom extended out from the back wall and divided the choice area into two equally-sized and distinct spatial locations. Each of these two locations

contained a ceramic ramequin (non-porous; 3,5 ×6 cm (depth; diameter)). A ramequin filled with water was placed in the starting area. Mice doing this test were food restricted to 85% of their *ad lib*. feeding weight in the days prior to testing. When stabilized at 85% of their *ad lib*. body weight, mice where trained and tested. Mice were on a 85% ad lib food restriction diet during the full duration of the experiment. The experiment was divided in three steps: Acclimation, Training and Testing. When chemogenetic activation was conducted, the rescue experiment included two additional sessions: Rescue and Validation.

Acclimation For 2–3 days, the mice were placed in the apparatus for 1 h with the middle door open. They were encouraged to explore the choice area by continuously filling the Ramequin with 1/8 pieces of Froot Loops cereals (Kellogg's, Battle Creek, MI).

Training On the subsequent day, the mice were placed in the start area with the middle door closed. Upon opening of the door, the mice had 3 min to reach the ramequin and eat the cereals. After that time, mice were guided toward the start area and the door was closed. Gradually, after each completed trials, bedding media was added into the ramequin in order to cover the food. Bedding media was added after each trial until the food reward was fully covered and the mouse reliably demonstrated the ability to dig in a full pot to find the food reward. Mice failing to demonstrate the ability to find food reward within 2 h were re-trained on the next day. Mice failing again to dig to find food were then excluded.

Testing Mice were tested in seven stages: Simple discrimination (SD), Compound Discrimination (CD), Compound Discrimination—Reversal (CDR), Intra-Dimensional Shift 1 to 3(IDS1, IDS2, IDS3) and Extra-dimensional shift (EDS). Following SD, media and scent were paired for each of the steps. Rewarding ramequin was placed randomly on the left or right side of the maze to avoid the use of spatial cues. Food reward was covered with scented (or not, in the case of SD) media and cereal dust was sprinkled on top of the media to avoid aberrant smell cues. To complete a trial, the mice had to dig into a media to retrieve the food reward. On incorrect trials, animals were free to visit the other side of the apparatus, but the other ramequin was removed. At the end of each trial, animals were guided to the start area and the ramequins were refilled or changed. Animals had 3 min to complete a trial and needed to succeed 8 trials out of 10 to advance to the next stage. The testing phase was scheduled on 2 days. SD, CD, CDR and IDS1 were performed on day 1, followed by IDS2, IDS3 and EDS on day 2.

Rescue PV^{Cre};$Cacna1a^{c/+}$ mutant and PV^{Cre} control mice injected with either AAV9.CAG.Flex.tdTomato.WPRE.bGH or 246-pAAV-hSYN-DIO-hM3D(Gq)-mCherry were tested for rescue by chemogenetic activation through the injection of CNO i.p. 30 min prior to testing. The rescue was reminiscent of the normal Attention Set Shifting task, to which was added 2 more days of testing (Supplementary Fig. 3) consisting of two IDS followed by an EDS. On day 3, mice were injected with 3 mg/kg CNO, 30 min before the first trial, and tested with 3 phases: IDS4, IDS5, EDS2. On day 4, mice were injected with vehicle, 30 min prior to the first trial, and underwent IDS6, IDS7 and EDS3. Of note, the trials on day 2 were also conducted following a vehicle injection 30 min prior to testing, in order to properly assess the impact of chemogenetic activation with CNO on day 3 (and exclude behavioural changes attributed to the injection itself).

Olfactory discrimination task Olfactory testing was conducted to ensure that mutant mice presented intact olfactory discrimination abilities (compared to control mice). The SD, CD and CDR of the Attention Set Shifting Task were recapitulated but odour, not media, was used as the relevant cue.

The following items were used for their different textures: paper, foam sheet, raffia, ribbon, pompom, plastic sheet, googly eyes, pipe cleaner, wooden beads, towel.

The following essential oils were used for their different odours: Balsam fir, lavender, lemon, ginger, cinnamon, clove, rosemary, anise, vanilla and thymus. One drop of oil (≈25 µl) was diluted in 500 µl of EtOH. Half rounded paper filter was scented with 25 µl of the EtOH-oil solution and put into the ramequin over night.

Probabilistic reversal learning task

This task was adapted from *Amodeo and al*. [28]. This experiment was performed in the apparatus used for the Attention Set Shifting task, although the dividing wall defining the choice area presented no sniffing holes. Each of these two locations contained a ceramic ramequin (non-porous; 3,5 × 6 cm (depth; diameter)). A ramequin filled with water was placed in the starting area. Mice were food restricted to 85% of their *ad lib*. feeding weight in the days prior to testing. When stabilized at 85% of their *ad lib*. body weight, mice where trained and tested.

Training step Mice were trained for 2–5 days before conducting the acquisition task. At the beginning of training, mice were first placed in the start area. The start door was opened and the mouse was free to navigate in the choice area and consume 1/8 of a piece of Froot Loops cereals (Kellogg's, Battle Creek, MI) from each food well. Once the cereal pieces were eaten from both compartments, the door was immediately opened to allow the mouse to return to the start area. If the mouse did not navigate back to

the start area within 5 s after consuming both cereal pieces, the experimenter gently nudged it back toward the start area. By the last session of training, all mice returned to the start area within 3–5 s after completing a trial without having to be handled by the experimenter. After returning to the start area, the door was closed and the mouse was restricted from entering the choice area. Subsequently, the food wells were re-baited and the start door opened to begin a new trial. This procedure continued until 15 min had elapsed. Acquisition testing was allowed once a mouse completed 4–6 trials within 15 min for 2 consecutive days.

Acquisition step This step was conducted the day following the completion of the trial step. At the beginning of the acquisition step, the mice were placed in the start area. The start doors were opened and the mice could choose to enter one of the two spatial locations. Once in the choice area, the sliding doors were closed again. In the acquisition and reversal phase, only one of the two food-wells, the left or the right one, was baited with a 1/8 piece of cereal in each trial. The correct (left or right side) food-well had 80% chances to have food where the incorrect-sided food-well was baited with food 20% of the time. When the right location was selected, the mouse could eat the cereal piece, the doors were opened again and subsequently closed when the mouse returned to the start area. Upon a non-rewarded choice, the mouse was allowed to navigate to the other spatial location after the baited food had been removed. The door was then opened, allowing the mouse to return to the start area. The acquisition criterion was achieved when a mouse completed 6 consecutive correct trials.

Reversal step This step was conducted the day following the acquisition step. Just prior to the reversal-learning step, each mouse completed a retention test. This was conducted to determine whether there was a difference in retaining the initially learned rule (spatial discrimination) between mouse strains. In addition, the retention test ensured that the current rule has been properly reinforced. Indeed, during the retention test, the mouse was rewarded 100% of the time for choosing the correct spatial location (as determined during the acquisition phase). Criterion was achieved when a mouse successfully chose the correct spatial location on 5 out of 6 trials. Subsequently, the reversal-learning task started and was conducted exactly as the acquisition phase, but with the reinforced spatial location placed in the opposite chamber (new rule). The criterion for the reversal-learning test was six consecutive correct trials. For the acquisition step, the number of trials taken to complete the task was calculated. For the reversal step, the trials to complete the task, the number of perseverative errors—the number of trials the mouse took before going to the new spatial location minus the first trial of the test during the reversal task—and the regressive errors—each time the mouse went back to the previously learned location following its first entrance in the correct location during the reversal task—were calculated. Finally, the choice made following an unrewarded incorrect trial was quantified.

Rescue PV^{Cre};$Cacna1a^{c/+}$ mice injected with 246-pAAV-hSYN-DIO-hM3D(Gq)-mCherry viruses were compared to PV^{Cre};$Cacna1a^{c/+}$ mice injected with AAV9.CAGGS.Flex.tdTomato.WPRE.bGH control viruses. The Reversal Learning Task was conducted as described above, but tested mice received a saline injection i.p. 30 min before the acquisition trials, and a CNO (3 mg/kg) injection i.p. 30 min before the reversal trials.

Histology

Mice brains were collected by microdissection after an intracardiac perfusion of 4% PFA, fixed in 4% PFA at room temperature for 1 h and cryoprotected overnight at 4 °C in a 30% sucrose PBS solution. They were then embedded in CryoMatrix and frozen on dry ice. Cryosections of 40 µm were collected with a cryostat for future staining and stored at 4 °C in phosphate buffer saline (PBS). Free floating slice were processed for immunohistochemistry. Briefly, the tissue was rinsed with PBS for 5 min. The tissue was then infused with a blocking solution of 10% goat serum and 1% Triton-10X in PBS, 1 h at room temperature. The tissue was then incubated with blocking solution and the adequate primary antibodies (anti-PV (Rabbit), 1:5000, Swant; anti-EGFP (Rat), 1:1000, VWR; anti-SST (Rabbit), 1:1000, Chemicon; anti-NeuN (Mouse), 1:1000, Millipore, overnight at 4 °C. The tissue was rinsed 3×10 min in PBS and incubated with blocking solution and the adequate secondary antibodies for 2 h at room temperature the following day (anti-Rabbit-594, 1:1000, Invitrogen; anti-Mouse-647, 1:1000, Life technologies; anti-Rat-488, 1:1000, Invitrogen). The tissue was finally rinsed in PBS 3 × 5 min, mounted on slides, cover slipped with Vectashield (Vector), sealed with nail polish and stored at 4 °C until imaging.

Cell quantification

Following immunostaining, the slices were imaged on a Leica SP8 confocal microscope with a 20x dry lens. Brain slices 2.80 to 2.00 mm and 2.00 to 1.50 anterior to bregma were used for quantification of the oFC and mPFC respectively. All PV- or EGFP- expressing cells in the oFC were manually quantified using a counting frame of 3 ×1 mm covering the oFC and a 1 ×2 mm covering the mPFC.

Video-EEG recordings

Surgeries were performed under isoflurane anesthesia (2% in O2, 0.8 L/min). Stainless steel unipolar electrodes (Plastic One, E363/3/SPC) were implanted in the somatosensory cortex and CA1 areas (AP/ML/DV: Cortex: −1.0/−1.5/−1 mm, CA1: −2 /−1.5 /−2.0 mm to bregma) and a twisted bipolar electrode (Plastic One, E363/3-2tw/SPC) was implanted in the contralateral hippocampus (AP/ML/DV: −2.0/−1.5/−2 mm to bregma), with a reference electrode over the cerebellum. A ground screw was placed in the occipital bone. Video-EEGs were recorded 48 h later at 2 kHz acquisition speed, filtered at HP 1 Hz and LP 70 Hz, and digitized using Cervello-NeuroMed (Blackrock Microsystems). Recording sessions were conducted continuously for 72 h from P60 onwards in $PV^{Cre};Cacna1a^{c/+}$ mutants and controls. Traces were visualized and annotated manually for movement artefacts and for potential epileptic activity (defined as trains of spikes, spike-waves or poly-spike discharges interrupting the background rhythms in the absence of movement artefact), as described before [10].

Seizure threshold

A 3 cm polyethylene tubing was connected to the blunt end of a cut 27 G needle metal part forming the vein needle as described previously by [87]. This montage was connected with a saline tubing, another 15 cm polyethylene tubing connected to the blunt end of a cut 27 G needle metal part and to a full 27 G needle. The saline tubing was connected to a 1 ml syringe and filled with saline. Mice where lightly anesthetized with isoflurane and their tail were warmed with warm water. The tail was slightly pinched and the needle was introduced in the caudal vein. Retrograde blood flow into the tubing and smooth saline injection would indicate a successful insertion. The needle was then fixed to the tail by carefully placing a short piece of microsurgical tape (3 M Micropore) around the tail at the point where the needle enters the vein. At that point, the isoflurane anesthesia was ceased and EEG recording was initiated. The 15 cm saline tubing was changed for the PTZ tubing, a 25 cm polyethylene tubing montage prefilled with PTZ (1%) and connected to a 1 ml PTZ syringe placed on a micro-infusion pump (Harvard Apparatus). Once the mice were awake (~3 min later), the infusion was initiated at a rate of 0.1 ml/min and continued until the first myoclonic twitch was observed and seizure activity was recorded. The PTZ tubing was then disconnected from the vein needle. Blood backflow in the still vein needle tube would confirm adequate placement of the needle post-hoc, as the contrary would suggest extravascular infusion. The amount of PTZ required to induce seizures (mg) was quantified and expressed over the weight of the mouse (kg) and compared between mice strains.

Statistical analysis

Statistical analysis of pooled data (means) from control and mutant mice were calculated with Prism (GraphPad, La Jolia, CA, USA). Bilateral Student's unpaired T-test was used where the data between two groups were normally distributed. Two Way Repeated Measures ANOVA followed by Bonferroni post-hoc test where used when multiple groups were compared. Kruskal-Wallis test or Mann-Whitney rank test was used when non-parametric analysis was required for non-normal data. Data are expressed as mean ± SEM and statistical significance was set as $p < 0.05$.

Minimal sample size required for each experimental paradigm was calculated using power analysis based on effect size established from previously published data [11, 88], with alpha = 0.05 and 1-beta = 0.95 (G*Power Software, version 3.1.9.4). We estimate that $n = 4$ mice per genotype for immunohistochemical cell counts, $n = 10$ cells (>3 mice/genotype) for in vitro electrophysiology, $n = 5$ mice per genotype for EEG result in >95% power to detect an effect size of >2, while $n = 10$ for behavioural assays detects an effect size >1.5 with 95% power (although for some behavioural experiments, a clear statistical difference was observed with $n = 5$–6 mice per genotype, which was then deemed sufficient).

Data availability

The datasets generated and/or analyzed during the current study are available from the corresponding author on reasonable request.

Acknowledgements We are grateful to the patients and families for their dedication and support towards our work. We acknowledge Ilse Riebe for preliminary data; J. Waldron, F. Boucher, D. Carrier and the animal facility personnel for their care of animals involved in this study. A. Van den Maagdenberg (U. Leiden), S. Arber (U. Basel) and G. Fishell (NYU, USA) generously donated various mouse lines. This work was supported by the Canadian Institutes for Health Research (CIHR, Grant MOP #119553 and PJT-391422 to ER; PJT-153311 to J-CL), the Fonds de la Recherche du Québec en Santé (FRQS; Groupe de Recherche sur le Système Nerveux Central [GRSNC] group grant, and Centre Interdisciplinaire de Recherche sur le Cerveau et l'Apprentissage [CIRCA] center grant, to J-CL). A. Lupien-Meilleur received MSc/PhD training awards from the CHU Ste-Justine Fondation des Étoiles and from the Department of Neuroscience, Université de Montréal. XJ received a post-doctoral training award from the Savoy Foundation. J-CL is the recipient of the Canada Research Chair in Cellular and Molecular Neurophysiology. ER receives a Clinician-scientist salary award from the Fonds de Recherche du Québec en Santé (FRQS) and a Young Investigator Award from the CIHR.

Author contributions AL-M, ER, and J-CL contributed to the conception and design of the study. AL-M, XJ, VT-D, LG, CV, and IR contributed to data acquisition and analysis. AL-M, XJ, ML, J-CL, and ER contributed to the manuscript preparation and editing. All authors approved the final version of the manuscript.

Compliance with ethical standards

Conflict of interest The authors declare no competing interest.

Publisher's note Springer Nature remains neutral with regard to jurisdictional claims in published maps and institutional affiliations.

References

1. Rajakulendran S, Kaski D, Hanna MG. Neuronal P/Q-type calcium channel dysfunction in inherited disorders of the CNS. Nat Rev Neurol. 2012;8:86–96.
2. Damaj L, Lupien-Meilleur A, Lortie A, Riou E, Ospina LH, Gagnon L, et al. CACNA1A haploinsufficiency causes cognitive impairment, autism and epileptic encephalopathy with mild cerebellar symptoms. Eur J Hum Genet. 2015;23:1505–12.
3. Epi KC. De novo mutations in SLC1A2 and CACNA1A are important causes of epileptic encephalopathies. Am J Hum Genet. 2016;99:287–98.
4. Auvin S, Holder-Espinasse M, Lamblin MD, Andrieux J. Array-CGH detection of a de novo 0.7-Mb deletion in 19p13.13 including CACNA1A associated with mental retardation and epilepsy with infantile spasms. Epilepsia. 2009;50:2501–03.
5. Reinson K, Oiglane-Shlik E, Talvik I, Vaher U, Ounapuu A, Ennok M, et al. Biallelic CACNA1A mutations cause early onset epileptic encephalopathy with progressive cerebral, cerebellar, and optic nerve atrophy. Am J Med Genet A. 2016;170:2173–6.
6. Jiang X, Raju PK, D'Avanzo N, Lachance M, Pepin J, Dubeau F, et al. Both gain-of-function and loss-of-function de novo CACNA1A mutations cause severe developmental epileptic encephalopathies in the spectrum of Lennox-Gastaut syndrome. Epilepsia. 2019;60:1881–94.
7. Humbertclaude V, Riant F, Krams B, Zimmermann V, Nagot N, Annequin D, et al. Cognitive impairment in children with CACNA1A mutations. Dev Med Child Neurol. 2020;62:330–7.
8. Catterall WA, Few AP. Calcium channel regulation and presynaptic plasticity. Neuron. 2008;59:882–901.
9. Jun K, Piedras-Renteria ES, Smith SM, Wheeler DB, Lee SB, Lee TG, et al. Ablation of P/Q-type Ca(2+) channel currents, altered synaptic transmission, and progressive ataxia in mice lacking the alpha(1A)-subunit. Proc Natl Acad Sci USA. 1999;96:15245–50.
10. Rossignol E, Kruglikov I, van den Maagdenberg AM, Rudy B, Fishell G. CaV 2.1 ablation in cortical interneurons selectively impairs fast-spiking basket cells and causes generalized seizures. Ann Neurol. 2013;74:209–22.
11. Jiang X, Lupien-Meilleur A, Tazerart S, Lachance M, Samarova E, Araya R, et al. Remodeled cortical inhibition prevents motor seizures in generalized epilepsy. Ann Neurol. 2018;84:436–51.
12. Maejima T, Wollenweber P, Teusner LU, Noebels JL, Herlitze S, Mark MD. Postnatal loss of P/Q-type channels confined to rhombic-lip-derived neurons alters synaptic transmission at the parallel fiber to purkinje cell synapse and replicates genomic Cacna1a mutation phenotype of ataxia and seizures in mice. J Neurosci. 2013;33:5162–74.
13. Todorov B, Kros L, Shyti R, Plak P, Haasdijk ED, Raike RS, et al. Purkinje cell-specific ablation of Cav2.1 channels is sufficient to cause cerebellar ataxia in mice. Cerebellum. 2012;11:246–58.
14. Mark MD, Maejima T, Kuckelsberg D, Yoo JW, Hyde RA, Shah V, et al. Delayed postnatal loss of P/Q-type calcium channels recapitulates the absence epilepsy, dyskinesia, and ataxia phenotypes of genomic Cacna1a mutations. J Neurosci. 2011;31:4311–26.
15. Siegle JH, Pritchett DL, Moore CI. Gamma-range synchronization of fast-spiking interneurons can enhance detection of tactile stimuli. Nat Neurosci. 2014;17:1371–9.
16. Carlen M, Meletis K, Siegle JH, Cardin JA, Futai K, Vierling-Claassen D, et al. A critical role for NMDA receptors in parvalbumin interneurons for gamma rhythm induction and behavior. Mol Psychiatry. 2012;17:537–48.
17. Cardin JA, Carlen M, Meletis K, Knoblich U, Zhang F, Deisseroth K, et al. Driving fast-spiking cells induces gamma rhythm and controls sensory responses. Nature. 2009;459:663–7.
18. Fuchs EC, Zivkovic AR, Cunningham MO, Middleton S, Lebeau FE, Bannerman DM, et al. Recruitment of parvalbumin-positive interneurons determines hippocampal function and associated behavior. Neuron. 2007;53:591–604.
19. Kim H, Ahrlund-Richter S, Wang X, Deisseroth K, Carlen M. Prefrontal parvalbumin neurons in control of attention. Cell. 2016;164:208–18.
20. Cho KK, Hoch R, Lee AT, Patel T, Rubenstein JL, Sohal VS. Gamma rhythms link prefrontal interneuron dysfunction with cognitive inflexibility in Dlx5/6(+/−) mice. Neuron. 2015;85:1332–43.
21. Bissonette GB, Schoenbaum G, Roesch MR, Powell EM. Interneurons are necessary for coordinated activity during reversal learning in orbitofrontal cortex. Biol Psychiatry. 2015;77:454–64.
22. Pi H-J, Hangya B, Kvitsiani D, Sanders JI, Huang ZJ, Kepecs A. Cortical interneurons that specialize in disinhibitory control. Nature. 2013;503:521–24.
23. Canetta S, Bolkan S, Padilla-Coreano N, Song LJ, Sahn R, Harrison NL, et al. Maternal immune activation leads to selective functional deficits in offspring parvalbumin interneurons. Mol Psychiatry. 2016;21:956–68.
24. Zaitsev AV, Povysheva NV, Lewis DA, Krimer LS. P/Q-type, but not N-type, calcium channels mediate GABA release from fast-spiking interneurons to pyramidal cells in rat prefrontal cortex. J Neurophysiol. 2007;97:3567–73.
25. Murray AJ, Woloszynowska-Fraser MU, Ansel-Bollepalli L, Cole KL, Foggetti A, Crouch B, et al. Parvalbumin-positive interneurons of the prefrontal cortex support working memory and cognitive flexibility. Sci Rep. 2015;5:16778.
26. Lee E, Lee J, Kim E. Excitation/Inhibition imbalance in animal models of autism spectrum disorders. Biol Psychiatry. 2017;81:838–47.
27. Korotkova T, Fuchs EC, Ponomarenko A, von Engelhardt J, Monyer H. NMDA receptor ablation on parvalbumin-positive interneurons impairs hippocampal synchrony, spatial representations, and working memory. Neuron. 2010;68:557–69.
28. Amodeo DA, Jones JH, Sweeney JA, Ragozzino ME. Differences in BTBR T+ tf/J and C57BL/6J mice on probabilistic reversal learning and stereotyped behaviors. Behav Brain Res. 2012;227:64–72.
29. Heisler JM, Morales J, Donegan JJ, Jett JD, Redus L, O'Connor JC. The attentional set shifting task: a measure of cognitive flexibility in mice. J Vis Exp. 2015.
30. Bomben VC, Aiba I, Qian J, Mark MD, Herlitze S, Noebels JL. Isolated P/Q calcium channel deletion in layer vi corticothalamic neurons generates absence epilepsy. J Neurosci. 2016;36:40518.
31. Mallmann RT, Elgueta C, Sleman F, Castonguay J, Wilmes T, van den Maagdenberg A, et al. Ablation of Ca(V)2.1 voltage-gated Ca(2)(+) channels in mouse forebrain generates multiple cognitive impairments. PLoS One. 2013;8:e78598.
32. Iwasato T, Datwani A, Wolf AM, Nishiyama H, Taguchi Y, Tonegawa S, et al. Cortex-restricted disruption of NMDAR1 impairs neuronal patterns in the barrel cortex. Nature. 2000;406:726–31.
33. Kim D, Jeong H, Lee J, Ghim J-W, Her ES, Lee S-H, et al. Distinct roles of parvalbumin- and somatostatin-expressing interneurons in working memory. Neuron. 2016;92:902–15.
34. Lak A, Costa GM, Romberg E, Koulakov AA, Mainen ZF, Kepecs A. Orbitofrontal cortex is required for optimal waiting based on decision confidence. Neuron. 2014;84:190–201.

35. Bissonette GB, Martins GJ, Franz TM, Harper ES, Schoenbaum G, Powell EM. Double dissociation of the effects of medial and orbital prefrontal cortical lesions on attentional and affective shifts in mice. J Neurosci. 2008;28:11124–30.
36. Bissonette GB, Bae MH, Suresh T, Jaffe DE, Powell EM. Prefrontal cognitive deficits in mice with altered cerebral cortical GABAergic interneurons. Behav Brain Res. 2013;259:143–51.
37. Manvich DF, Webster KA, Foster SL, Farrell MS, Ritchie JC, Porter JH, et al. The DREADD agonist clozapine N-oxide (CNO) is reverse-metabolized to clozapine and produces clozapine-like interoceptive stimulus effects in rats and mice. Sci Rep. 2018;8:3840.
38. Indelicato E, Nachbauer W, Karner E, Eigentler A, Wagner M, Unterberger I, et al. The neuropsychiatric phenotype in CACNA1A mutations: a retrospective single center study and review of the literature. Eur J Neurol. 2019;26:66–e67.
39. Hamdan FF, Myers CT, Cossette P, Lemay P, Spiegelman D, Laporte AD, et al. High rate of recurrent de novo mutations in developmental and epileptic encephalopathies. Am J Hum Genet. 2017;101:664–85.
40. Fletcher CF, Lutz CM, O'Sullivan TN, Shaughnessy JD Jr., Hawkes R, Frankel WN, et al. Absence epilepsy in tottering mutant mice is associated with calcium channel defects. Cell. 1996;87:607–17.
41. Fletcher CF, Tottene A, Lennon VA, Wilson SM, Dubel SJ, Paylor R, et al. Dystonia and cerebellar atrophy in Cacna1a null mice lacking P/Q calcium channel activity. FASEB J. 2001;15:1288–90.
42. Alonso I, Marques JM, Sousa N, Sequeiros J, Olsson IA, Silveira I. Motor and cognitive deficits in the heterozygous leaner mouse, a Cav2.1 voltage-gated $Ca2^{+}$ channel mutant. Neurobiol Aging. 2008;29:1733–43.
43. Takahashi E, Niimi K, Itakura C. Motor coordination impairment in aged heterozygous rolling Nagoya, Cav2.1 mutant mice. Brain Res. 2009;1279:50–7.
44. Takahashi E, Niimi K, Itakura C. Age-related spatial and non-spatial short-term memory in Cav2.1alpha1 mutant mice, Rolling Nagoya. Behav Brain Res. 2009;204:241–5.
45. Jacobi H, du Montcel ST, Bauer P, Giunti P, Cook A, Labrum R, et al. Long-term disease progression in spinocerebellar ataxia types 1, 2, 3, and 6: a longitudinal cohort study. Lancet Neurol. 2015;14:1101–8.
46. Jiang X, Lachance M, Rossignol E. Involvement of cortical fast-spiking parvalbumin-positive basket cells in epilepsy. Prog Brain Res. 2016;226:81–126.
47. Rossignol E. Genetics and function of neocortical GABAergic interneurons in neurodevelopmental disorders. Neural Plast. 2011;2011:649325.
48. Holmes GL. Cognitive impairment in epilepsy: the role of network abnormalities. Epileptic Disord. 2015;17:101–16.
49. Dutton SB, Makinson CD, Papale LA, Shankar A, Balakrishnan B, Nakazawa K, et al. Preferential inactivation of Scn1a in parvalbumin interneurons increases seizure susceptibility. Neurobiol Dis. 2012;49C:211–20.
50. Yu FH, Mantegazza M, Westenbroek RE, Robbins CA, Kalume F, Burton KA, et al. Reduced sodium current in GABAergic interneurons in a mouse model of severe myoclonic epilepsy in infancy. Nat Neurosci. 2006;9:1142–9.
51. Han S, Tai C, Westenbroek RE, Yu FH, Cheah CS, Potter GB, et al. Autistic-like behaviour in Scn1a+/− mice and rescue by enhanced GABA-mediated neurotransmission. Nature. 2012;489:385–90.
52. Cheah CS, Yu FH, Westenbroek RE, Kalume FK, Oakley JC, Potter GB, et al. Specific deletion of NaV1.1 sodium channels in inhibitory interneurons causes seizures and premature death in a mouse model of Dravet syndrome. Proc Natl Acad Sci USA. 2012;109:14646–51.
53. Chao HT, Chen H, Samaco RC, Xue M, Chahrour M, Yoo J, et al. Dysfunction in GABA signalling mediates autism-like stereotypies and Rett syndrome phenotypes. Nature. 2010;468:263–9.
54. Flames N, Long JE, Garratt AN, Fischer TM, Gassmann M, Birchmeier C, et al. Short- and long-range attraction of cortical GABAergic interneurons by neuregulin-1. Neuron. 2004;44:251–61.
55. Li KX, Lu YM, Xu ZH, Zhang J, Zhu JM, Zhang JM, et al. Neuregulin 1 regulates excitability of fast-spiking neurons through Kv1.1 and acts in epilepsy. Nat Neurosci. 2012;15:267–73.
56. Fazzari P, Paternain AV, Valiente M, Pla R, Lujan R, Lloyd K, et al. Control of cortical GABA circuitry development by Nrg1 and ErbB4 signalling. Nature. 2010;464:1376–80.
57. Chen YJ, Zhang M, Yin DM, Wen L, Ting A, Wang P, et al. ErbB4 in parvalbumin-positive interneurons is critical for neuregulin 1 regulation of long-term potentiation. Proc Natl Acad Sci USA. 2010;107:21818–23.
58. Woo RS, Li XM, Tao Y, Carpenter-Hyland E, Huang YZ, Weber J, et al. Neuregulin-1 enhances depolarization-induced GABA release. Neuron. 2007;54:599–610.
59. Wen L, Lu YS, Zhu XH, Li XM, Woo RS, Chen YJ, et al. Neuregulin 1 regulates pyramidal neuron activity via ErbB4 in parvalbumin-positive interneurons. Proc Natl Acad Sci USA. 2010;107:1211–16.
60. Del Pino I, Garcia-Frigola C, Dehorter N, Brotons-Mas JR, Alvarez-Salvado E, Martinez de Lagran M, et al. Erbb4 deletion from fast-spiking interneurons causes schizophrenia-like phenotypes. Neuron. 2013;79:1152–68.
61. Tan GH, Liu YY, Hu XL, Yin DM, Mei L, Xiong ZQ. Neuregulin 1 represses limbic epileptogenesis through ErbB4 in parvalbumin-expressing interneurons. Nat Neurosci. 2012;15:258–66.
62. Yizhar O, Fenno LE, Prigge M, Schneider F, Davidson TJ, O'Shea DJ, et al. Neocortical excitation/inhibition balance in information processing and social dysfunction. Nature. 2011;477:171–8.
63. Sohal VS, Rubenstein JLR. Excitation-inhibition balance as a framework for investigating mechanisms in neuropsychiatric disorders. Mol Psych. 2019;24:1248–57.
64. Powell EM, Campbell DB, Stanwood GD, Davis C, Noebels JL, Levitt P. Genetic disruption of cortical interneuron development causes region- and GABA cell type-specific deficits, epilepsy, and behavioral dysfunction. J Neurosci. 2003;23:622–31.
65. Levitt P, Eagleson KL, Powell EM. Regulation of neocortical interneuron development and the implications for neurodevelopmental disorders. Trends Neurosci. 2004;27:400–6.
66. Freund TF, Katona I. Perisomatic inhibition. Neuron. 2007;56:33–42.
67. Bartos M, Vida I, Jonas P. Synaptic mechanisms of synchronized gamma oscillations in inhibitory interneuron networks. Nat Rev Neurosci. 2007;8:45–56.
68. Sohal VS, Zhang F, Yizhar O, Deisseroth K. Parvalbumin neurons and gamma rhythms enhance cortical circuit performance. Nature. 2009;459:698–702.
69. Howard MW, Rizzuto DS, Caplan JB, Madsen JR, Lisman J, Aschenbrenner-Scheibe R, et al. Gamma oscillations correlate with working memory load in humans. Cereb Cortex. 2003;13:1369–74.
70. Lopez-Pigozzi D, Laurent F, Brotons-Mas JR, Valderrama M, Valero M, Fernandez-Lamo I, et al. Altered oscillatory dynamics of CA1 parvalbumin basket cells during theta-gamma rhythmopathies of temporal lobe epilepsy. eNeuro. 2016;3.
71. Llinás RR, Choi S, Urbano FJ, Shin H-S. Gamma-band deficiency and abnormal thalamocortical activity in P/Q-type channel mutant mice. Proc Natl Acad Sci USA. 2007;104:17819–24.
72. Roth BL. DREADDs for neuroscientists. Neuron. 2016;89:683–94.
73. Wechsler D. WISC-IV Administration and Scoring Manual. PsychCorp; San Antonio, TX; 2003.

74. Wechsler D. WISC-IV Technical and Interpretative Manual. PsychCorp; San Antonio, TX; 2003.
75. Conners CK. Conner's Rating Scale, 3rd Edition. Toronto, Ontario; Multi-Health Systems; New York: 2008.
76. Delis DC, Kaplan E, Kramer JH. Delis-Kaplan Executive Function System™ (D-KEFS™). Standardized test purchasable at Pearson's; London, UK; 2001.
77. Shallice T. Specific impairments of planning. Philos Trans R Soc Lond B Biol Sci. 1982;298:199–209.
78. Manley Tea. Test of Everyday Attention for Children, The (TEA-Ch). Standardized test purchasable at Pearson's; London, UK; 1998.
79. Wechsler D Wechsler Memory Scale - Fourth Edition (WMS-IV). Standardized test purchasable at Pearson's; London, UK; 2009.
80. Beery KE, Buktenica NA, Beery NA Beery-Buktenica Developmental Test of Visual-Motor Integration, Sixth Edition, The (BEERY™ VMI). Standardized test purchasable at Pearson's; London, UK; 2010.
81. Instrument L Purdue Pegboard Test Manual. Standardized test purchasable at lafayette instrument; Lafayette, IN, USA; 2002.
82. Martin NA, Brownell R EOWPVT-4: Expressive One-Word Picture Vocabulary Test–Fourth Edition. WPS; Torrance, CA; 2010.
83. Kuhlman SJ, Huang ZJ. High-resolution labeling and functional manipulation of specific neuron types in mouse brain by Cre-activated viral gene expression. PLoS One. 2008;3:e2005.
84. Todorov B, van de Ven RC, Kaja S, Broos LA, Verbeek SJ, Plomp JJ, et al. Conditional inactivation of the Cacna1a gene in transgenic mice. Genesis. 2006;44:589–94.
85. Sousa VH, Miyoshi G, Hjerling-Leffler J, Karayannis T, Fishell G. Characterization of Nkx6-2-derived neocortical interneuron lineages. Cereb Cortex. 2009;19:i1–10.
86. Haji N, Riebe I, Aguilar-Valles A, Artinian J, Laplante I, Lacaille JC. Tsc1 haploinsufficiency in Nkx2.1 cells upregulates hippocampal interneuron mTORC1 activity, impairs pyramidal cell synaptic inhibition, and alters contextual fear discrimination and spatial working memory in mice. Mol Autism. 2020;11:29.
87. Töllner K, Twele F, Löscher W. Evaluation of the pentylenetetrazole seizure threshold test in epileptic mice as surrogate model for drug testing against pharmacoresistant seizures. Epilepsy Behav. 2016;57:95–104.
88. Patel JC, Rossignol E, Rice ME, Machold RP. Opposing regulation of dopaminergic activity and exploratory motor behavior by forebrain and brainstem cholinergic circuits. Nat Commun. 2012;3:1172.